Title: Binucleated cells generated by nuclear movement during neural transdifferentiation from human bone marrow-derived mesenchymal cells

Authors: Carlos Bueno[1,*], Miguel Blanquer[1], David García-Bernal[1,2], Salvador Martínez[3] and José M. Moraleda[1].

[1]Medicine Department and Hematopoietic Transplant and Cellular Therapy Unit, Institute of Biomedical Research (IMIB), University of Murcia, Faculty of Medicine, Murcia, 30120, Spain.

[2]Biochemistry, Molecular Biology and Immunology Department, University of Murcia, Faculty of Medicine, Murcia, 30100, Spain

[3]Instituto de Neurociencias de Alicante (UMH-CSIC), Universidad Miguel Hernandez, San Juan, Alicante, 03550, Spain.

*Correspondence: Carlos Bueno, PhD., Medicine Department and Hematopoietic Transplant and Cellular Therapy Unit, Institute of Biomedical Research (IMIB), University of Murcia, Faculty of Medicine, Murcia, 30120, Spain. Tel.: 0034-968885013. Fax: 00-34-868884150. E-mail: carlos.bueno@um.es

Abstract

Although it has been reported that bone marrow-derived cells (BMDCs) can transdifferentiate into neural cells, the findings are considered unlikely. It has been argued that the rapid neural transdifferentiation of BMDCs reported in culture studies is actually due to cytotoxic changes induced by the media. While transplantation studies indicated that BMDCs can form new neurons, it remains unclear whether the underlying mechanism is transdifferentiation or BMDCs-derived cell fusion with the existing neuronal cells. Cell fusion has been put forward to explain the presence of gene-marked binucleated neurons after gene-marked BMDCs transplantation. In the present study, we demostrated that human BMDCs can rapidly adopt a neural-like morphology through active neurite extension and binucleated human BMDCs can form with independence of any cell fusion events. We also showed that BMDCs neural transdifferentiation involves the formation of intermediate cells which can then redifferentiate into neural-like cells, redifferentiate back to the mesenchymal fate or even repeatedly switch lineages without cell division. Furthermore, we have discovered that nuclei from intermediate cells rapidly move within the cell, adopting different morphologies and even forming binucleated cells. Therefore, our results provide a stronger basis for rejecting the idea that BMDCs neural transdifferentiation is merely an artefact.

46 # Introduction

47 The fate of adult cells has been thought to be restricted to their tissues of origin
48 (Waddington, 1957). However, recent studies have indicated that certain mammalian
49 adults cells may be more plastic than we previously thought in that they maintain the
50 ability for multilineage cell differentiation and may turn into cells of unrelated lineages,
51 a phenomenon known as adult cell plasticity (Blau et al., 2001; Raff et al., 2003; Jopling
52 et al., 2011; Merrell et al., 2016; Rajagopal et al., 2016). The first suggestion that adult
53 cells switch into another cell type of an unrelated tissue came from studies of whole bone
54 marrow transplantation in humans and animal models. These studies suggested that bone
55 marrow-derived cells (BMDCs) could enter the brain and transdifferentiate into cells with
56 a neuronal-specific phenotype (Brazelton et al., 2000; Mezey et al, 2000; Mezey et al,
57 2003). Bone marrow contains two prototypical stem cell population: haematopoietic stem
58 cells (HSCs) and mesenchymal stromal cells (MSCs). Whereas HSCs give rise to the
59 various blood cells, bone marrow-derived MSCs can differentiate into mesodermal
60 lineage cells such as osteocytes, chondrocytes, and adipocytes (Grove et al, 2004).
61 Nevertheless, several reports have indicated that BMDCs and MSCs isolated from
62 different adult tissues can also transdifferentiate into neural cells, both in vitro (Woodbury
63 et al., 2000; Woodbury et al., 2002; Muñoz-Elias et al., 2003; Jeong et al., 2004; Suon et
64 al., 2004; Hermann et al., 2006; Ning et al., 2006; Bueno et al., 2013; Azedi et al., 2017;
65 Radhakrishnan et al., 2019) and in vivo (Azizi et al., 1998; Kopen et al., 1999; Brazelton
66 et al., 2000; Mezey et al, 2000; Priller et al., 2001; Mezey et al, 2003; Muñoz-Elias et al.,
67 2004; Nern et al, 2009; Bueno et al., 2013). However, the findings and their interpretation
68 have been challenged (Krabbe et al., 2005; Kemp et al., 2014). The main argument against
69 these observations in culture studies is that MSCs rapidly adopt neural-like morphologies
70 through retraction of the cytoplasm, rather than by active neurite extension (Krabbe et al.,

71 2005; Neuhuber et al., 2004; Lu et al., 2004; Bertani et al., 2005). While transplantation
72 studies have indicated that BMDCs can contribute to the neuronal architecture of the
73 nervous system, including Purkinje cells within the cerebellum (Brazelton et al., 2000;
74 Mezey et al, 2000; Priller et al., 2001; Mezey et al, 2003; Muñoz-Elias, G et al., 2004;
75 Nern et al, 2009), the possibility of BMDCs transdifferenting into neural cells is
76 considered unlikely, and the more accepted explanation that donor BMDCs fuse with host
77 neurons (Kemp et al., 2014). Cell fusion has been put forward to explain the presence of
78 gene-marked binucleated Purkinje neurons after gene-marked bone marrow-derived cell
79 transplantation (Alvarez-Dolado et al., 2003; Weimann et al., 2003). The actual
80 occurrence of neuronal transdifferentiation of BMDCs and MSCs is currently much
81 debated, but would have immense clinical potential in cell replacement therapy of
82 neurodegenerative diseases (Hernández et al., 2020).

83 We recently reported that MSCs isolated from adult human tissues (hMSCs) can
84 transdifferentiate into neural-like cells without passing through a mitotic stage and that
85 they shrank dramatically and changed their morphology to that of neural-like cells
86 through active neurite extensión (Bueno et al., 2019; Bueno et al., 2021). These findings
87 support the notion that the transdifferentiation of hMSCs towards a neural-like lineage
88 involves a dedifferentiation event prior to re-differentiation to neural-like phenotypes,
89 thus definitively confirming that the rapid acquisition of a neural-like morphology during
90 hMSC transdifferentiation is via a transdifferentiation trait rather than merely an artefact.
91 Furthermore, we noted that nuclear remodelling occurred during in vitro neural
92 transdifferentiation from hMSCs. We discovered that many hMSCs exhibit unusual
93 nuclear structures and even possess two nuclei.

94 In the present study, we examined the sequence of biological events during neural
95 transdifferentiation of human BM-MSCs (hBM-MSCs) by live-cell nucleus fluorescence

96 labelling and time-lapse microscopy to determine whether the binucleation events
97 observed during neural transdifferentiation from hMSCs are due to cell division or cell
98 fusion events.

99

100 # Results

101 **Morphological changes in hBM-MSCs during neural transdifferentiation**

102 We examined the sequence of biological events during neural transdifferentiation of
103 histone H2B-GFP transfected hBM-MSCs by time-lapse microscopy. Time-lapse
104 imaging revealed that, after neural induction, hBM-MSCs can rapidly reshape from a flat
105 to a spherical morphology. Subsequently, we observed that hMSC-derived round cells
106 can maintain the spherical shape (Figure 1, green arrows; video 1) or assume new
107 morphologies; round cells can change to a morphology similar to that of neural-like cells
108 through active neurite extension (Figure 1, red arrows; video 1) or they can revert back
109 to the mesenchymal morphology (Figure 1, yellow arrows; video 1).

110 The hBM-MSCs did not transdifferentiate at the same time or rate, so the cell culture
111 simultaneously contained hBM-MSCs at different stages of transdifferentiation.
112 Importantly, there was no cell proliferation or cell fusion through transdifferentiation
113 from hBM-MSCs (Figure 1; video 1). These results confirm our previous findings (Bueno
114 et al., 2019; Bueno et al., 2021) and lend further support to the notion that MSCs
115 transdifferentiate towards a neural lineage through a dedifferentiation step followed by
116 re-differentiation to neural phenotypes.

117 As noted above, hBM-MSC-derived round cells can even preserve their spherical
118 morphology for days without assuming new fates. However, it is important to note that

119 cellular protrusions appeared, moved and disappeared from the surface of hBM-MSC-
120 derived round cells during this dedifferentiation stage (Figure 2; video 2). Contrastingly,
121 we also found that hBM-MSC-derived round cells can adopt a neural-like morphology
122 via active neurite extension. (Figure 3; video 3). New neurites grew from the body of
123 some round cells, which gradually adopted a more complex morphology, by acquiring
124 dendrite-like (Figure 3, green arrows) and axon-like domains (Figure 3, yellow arrows).
125 We did not observe any cellular protrusions as hBM-MSC-derived round cells gradually
126 acquired a neural-like morphology. Finally, hBM-MSC-derived round and neural-like
127 cells could also re-differentiate back to the mesenchymal morphology (Figures 1-3;
128 videos 1-3). Surprisingly, hBM-MSCs could also rapidly and repeatedly switch lineages
129 without cell division (Figure 4; video 4). This finding is consistent with a previous study
130 that report Schwann cells can undergo multiple cycles of differentiation and
131 dedifferentiation without entering the cell cycle (Monje et al., 2010).

132 **Nuclear remodelling during neural transdifferentiation from hBM-MSCs**

133 Live-cell nucleus fluorescence labelling and time-lapse microscopy revealed that nuclear
134 remodelling occurred during neural transdifferentiation from hBM-MSCs. Nuclei from
135 histone H2B-GFP-expressing, hBM-MSC-derived round cells moved within the cell,
136 adopting different morphologies and positions, and even forming lobed nuclei (Figure 5;
137 video 5). Although the cell nuclei switched their morphologies while moving, the nuclear
138 movement primarily produces three different nuclear morphologies and positions. Firstly,
139 the cell nucleus acquired a finger-like shape and moves within the cell, generating the
140 cellular protrusions that appeared and disappeared from the surface of hBM-MSC-derived
141 round cells (Figure 6; video 6). Secondly, the nucleus acquired a finger-like shape, before
142 reorienting towards a peripheral position within the cell and acquiring a kidney-like
143 shape. Subsequently, the cell nucleus began to move rapidly around the cell (Figure 7;

144 video 7). And thirdly, the nucleus acquired a finger-like shape and moved within the cell
145 to form lobed nuclei connected by nucleoplasmic bridges. The lobed nuclei movement
146 also generated transient cellular protrusions on the surface of hBM-MSC-derived round
147 cells (Figure 8; video 8).

148 It is important to note that histone H2B-GFP-expressing, hBM-MSC-derived round cells
149 position their nucleus at the front of the cell during migration (Figure 9; videos 9 and 10).
150 This nuclear positioning was observed in mononucleated hBM-MSC-derived round cells,
151 in both cells with kidney shaped nuclei (Figure 9A; video 9) and cells with finger shaped
152 nuclei (Figure 9B; video 10). hBM-MSC-derived round cells with lobed nuclei also
153 positioned their nucleus at the front of the cell during migration (Figure 10A; video 11).
154 Furthermore, we observed that hBM-MSC-derived round cells with lobed nuclei
155 positioned their largest lobe at the front of the cell during migration (Figure 10B; video
156 12). These finding are consistent with a previous study that reported that human
157 leukocytes position their nucleus at the front of the cell during migration (Barzilai et al.,
158 2010).

159 As mentioned previously, hBM-MSC-derived round cells can also assume new
160 morphologies, gradually adopting a neural-like morphology through active neurite
161 extension or re-differentiating back to their mesenchymal morphology. There were no
162 changes in nuclear positioning or lobed nuclei formation as histone H2B-GFP-expressing,
163 hBM-MSC-derived round cells gradually acquired a neural-like morphology (Figure 11;
164 video 13). By contrast, when histone H2B-GFP-expressing, hBM-MSC-derived round
165 cells reverted back to the mesenchymal morphology, the nuclei from mononucleated
166 round cells gradually adopted their original ellipsoid shape (Figure 12A; video 14). Yet
167 when round cells with lobed nuclei reverted back to the mesenchymal morphology, the
168 lobed nuclei preserved their shape for hours (Figure 12B; video 15). In future studies,

169 live-cell nucleus fluorescence labelling and time-lapse microscopy over longer periods is
170 necessary to determine whether the lobed nuclei finally fused to form a single nucleus.

171 Finally, laser scanning confocal microscopy revealed that many histone H2B-GFP-
172 expressing, hBM-MSC-derived round cells with unusual nuclear structures also exhibited
173 extranuclear chromatin-containing bodies in the cellular cytoplasm during neural
174 transdifferentiation (Figure 13). We observed that hBM-MSCs with finger shaped nuclei
175 (Figure 13A), kidney shaped nuclei (Figure 13B) and lobed nuclei connected by
176 nucleoplasmic bridges (Figure 13C) can also exhibit extranuclear bodies in the cellular
177 cytoplasm. Furthermore, we found chromatin-containing bodies connected to the main
178 body of the nucleus by thin strands of nuclear material (Figure 13D), chromatin-
179 containing bodies moving away from or toward the main nuclei (Figure 13E) and two
180 lobed nuclei unconnected by any nucleoplasmic bridges with chromatin-containing
181 bodies in the cellular cytoplasm (Figure 13F). These results indicate that binucleated
182 hBM-MSCs form during neural transdifferentiation with independence of any cell
183 division or fusion events.

184 Importantly, the nuclear morphology of hBM-MSCs observed during the
185 transdifferentiation bears a lot of similarities to the nuclear morphology of neural stem
186 cells located in the ventricular-subventricular zone of the anterolateral ventricle wall of
187 the human foetal brain (Guerrero-Cázares et al., 2011) and adult mouse brain (Doetsch et
188 al., 1997; Capilla-Gonzalez et al., 2014; Cebrián-Silla et al., 2017); their nuclear
189 morphology is also very similar to that of many cultured hippocampal neurons (Wittmann
190 et al., 2009). For example, the nuclear morphologies in Figure 13C are very similar to
191 those observed in Wittmann et al. (2019, Fig. S2), Cebrián-Silla et al. (2017, Figs. 1E, 4I,
192 6F, S1B, S2B and S6A), Guerrero-Cázares et al. (2011, Fig. 2C) and Doetsch et al. (1997,
193 Fig. 3A). Furthermore, the nuclear morphologies shown in Figure 13D closely resemble

194 those reported by Cebrián-Silla et al. (2017, Figs. 1A,1B,1M,1N, 3I, 6A, 6B and 6H) and
195 Guerrero-Cázares et al (2011, Fig. 3j). In addition, the nuclear morphologies in Figure
196 13E are very similar to those observed in Capilla-Gonzalez et al. (2014, Fig. S2C).
197 Although it has been suggested that these unusual nuclear structures are associated with
198 quiescence in adult neural stem cells (Cebrián-Silla et al., 2017), our results suggest that
199 they are associated with nuclear movement within the cell during neuronal differentiation,
200 but without any relation to cell division.

201

202 **Discussion**

203 In this study, we have shown that when hBM-MSCs were exposed to a neural induction
204 medium, they rapidly reshaped from a flat to a spherical morphology. Subsequently,
205 hBM-MSC-derived round cells could preserve this the spherical morphology or assume
206 new ones; they gradually adopted a neural-like morphology through active neurite
207 extension or re-differentiated back to the mesenchymal fate. Furthermore, we found that
208 hBM-MSCs can rapidly and repeatedly switch lineages without cell division. Importantly,
209 there was no cell proliferation or cell fusion through transdifferentiation from hBM-
210 MSCs. This work also highlights that nuclear remodelling occurred during in vitro neural
211 transdifferentiation from hMSCs. We discovered that nuclei in intermediate cells rapidly
212 moved within the cell, adopting different morphologies and even forming lobed nuclei.
213 These nuclear movements generated transient cellular protrusions that appeared and
214 disappeared from the surface of hBM-MSC-derived round cells. The intermediate cells
215 positioned their nucleus at the front of the cell during migration.

216 The literature published in recent decades has shown that MSCs isolated from different
217 adult tissues can rapidly transdifferentiated into neural-like cells in culture (Woodbury et

218 al., 2002; Muñoz-Elias et al., 2003; Jeong et al., 2004; Suon et al., 2004; Ning et al., 2016;
219 Azedi et al., 2017; Radhakrishnan et al., 2019). However, the findings and their
220 interpretation have been challenged. It has been argued that the rapid neural
221 transdifferentiation of MSCs reported in culture studies is actually due to cytotoxic
222 changes induced by the media (Krabbe et al., 2005; Neuhuber et al., 2004; Lu et al., 2004
223 Bertani et al., 2005), so the rapid changes should not be interpreted as signs of
224 transdifferentiation. In this study, we have shown that hBM-MSCs can rapidly adopt a
225 neural-like morphology via active neurite extension. New neurites grew from the body of
226 some round cells, which gradually adopted a more complex morphology, by acquiring
227 dendrite-like and axon-like domains. These result confirm our previous findings (Bueno
228 et al., 2019; Bueno et al., 2021) and provide a stronger basis for rejecting the idea that the
229 rapid acquisition of a neural-like morphology during MSC transdifferentiation is merely
230 an artefact.

231 As mentioned previously, hBM-MSC-derived round cells (intermediate cells) could also
232 re-differentiated back to the mesenchymal fate. Furthermore, we found that hBM-MSCs
233 can rapidly and repeatedly switch lineages without cell division. It has been claimed that
234 the rapidity with which the neuron-like morphology is both gained and lost also argues
235 againts physiological differentiation (Phinney and Prockop, 2007). However, a recent
236 study has demostrated that Schwann cells can also rapidly undergo multiple cycles of
237 differentiation and dedifferentiation without entering the cell cycle (Monje et al., 2010).

238 While transplantation studies indicated that BMDCs and MSCs can contribute to the
239 neuronal architecture of the central nervous system, including that of Purkinje cells within
240 the cerebellum (Brazelton et al., 2000; Mezey et al, 2000; Priller et al., 2001; Mezey et
241 al, 2003; Muñoz-Elias, G et al., 2004; Nern et al, 2009; Bueno et al., 2013), it remains
242 unclear whether the underlying mechanism is transdifferentiation or BMDC fusion with

243 the existing neuronal cells, or both (Kemp et al., 2014). Cell fusion has been put forward
244 to explain the presence of gene-marked binucleated Purkinje neurons after gene-marked
245 bone marrow-derived cell transplantation (Alvarez-Dolado et al., 2003; Weimann et al.,
246 2003). Evidence supporting cell fusion derived from experiment using Cre/lox
247 recombination to detect fusion events (Alvarez-Dolado et al., 2003). Bone marrow cells
248 expressing both GFP and Cre recombinase where grafted in R26R mice. The study
249 confirmed the presence of two independent nuclei in a LacZ-positive and GFP-negative
250 Purkinje cell, but did not show any LacZ-positive and GFP-positive binucleated Purkinje
251 cell. Therefore, this study does not conclusively demonstrate that cell fusion is the
252 underlying mechanism to explain the presence of binucleated Purkinje neurons after bone
253 marrow-derived cell transplantation. Futher support to cell fusion came from experiment
254 using GFP-positive sex-mis-matched bone marrow transplants in mice (Weimann et al.,
255 2003). GFP-positive Purkinje cells where shown to contain two nuclei, with one of these
256 nuclei containing the Y chromosome. This study does not conclusively demonstrate that
257 GFP-positive Purkinje neurons found in the host cerebellum are the result of fusion
258 between a host female Purkinje cell and a male bone marrow-derived cells, only
259 demonstrates that binucleated Purkinje cells express markers of donor origin.

260 In this study, we demonstrated that binucleated hBM-MSCs can be formed during
261 transdifferentiation with independence of any cell fusion. Therefore, our results provide
262 evidence that transdifferentiation may be also the mechanism behind the presence of
263 gene-marked binucleated Purkinje neurons after gene-marked bone marrow-derived cell
264 transplantation.

265 It is important to note that binucleated Purkinje neurons are also present in healthy,
266 unmanipulated mice (Magrassi et al., 2007). Futhermore, human studies have also found
267 binucleated Purkinje neurons in non-transplanted individuals (Kemp et al., 2014). What

268 is more, many authors have reported binucleated neurons in various central and peripheral
269 parts of the nervous system including, the cerebral cortex, cerebellum, sympathetic and
270 spinal ganglia, diencephalon, midbrain, hindbrain, cerebral cortex and spinal cord
271 (Altman et al., 1963; Das et al., 1977, Ribak and Seress, 1983; Portiansky et al., 2006).

272 As mentioned previously, the nuclear morphology of hBM-MSCs observed during the
273 transdifferentiation bears a lot of similarities to the nuclear morphology of neural stem
274 cells located in the ventricular-subventricular zone of the anterolateral ventricle wall of
275 the human foetal brain (Guerrero-Cázares et al., 2011) and adult mouse brain (Doetsch et
276 al., 1997; Capilla-Gonzalez et al., 2014; Cebrián-Silla et al., 2017); their nuclear
277 morphology is also very similar to that of many cultured hippocampal neurons (Wittmann
278 et al., 2009). Although it has generally been believed that adult neurogenesis occurs
279 progressively through sequential phases of proliferation and neuronal differentiation of
280 adult stem cells (Bond et al., 2015), the approaches used to probe stem cell division and
281 differentiation, and even direct lineage tracing, are inherently limited (Rakic et al., 2002;
282 Cooper-Kuhn et al., 2002; Breunig et al., 2007; Kuhn et al., 2016; Sorrells et al., 2021).
283 These findings indicate that there is a lack of a reliable definitive method to label dividing
284 progenitors and follow their progeny (Sorrells et al., 2021). It is important to note that
285 almost none of reports describing newborn neurons in the adult brain have showed mitotic
286 figures which would confirm that adult neurogenesis occurs progressively through
287 sequential phases of proliferation (Doetsch et al., 1997; Doetsch et al., 1999a; Doetsch et
288 al., 1999b; Seri et al., 2001; Filippov et al., 2003; Kronenberg et al, 2003; Seri et al., 2004;
289 Kempermann et al., 2004). Collectively, these findings suggest the possibility that new
290 neurons can also be generated without necessitating cell division. Future research is
291 required to determine the likelihood of this premise.

292 The most important discovery in this work is the observation that nuclei in intermediate
293 cells rapidly move within the cell, adopting different morphologies and even forming
294 binucleated cells. This is the first direct evidence, to our knowledge, that the nucleus of a
295 human cell can change morphology and position so quickly. These nuclear movements
296 generated transient cellular protrusions that appeared and disappeared from the surface of
297 intermediate cells. Futhermore, the intermediate cells positioned their nucleus at the front
298 of the cell during migration. These findings may suggest that nuclei in intermediate cells
299 are somehow sensing their surroundings. Future research is required to determine the
300 feasibility of this conjecture. This study not only shows that the main nuclei move within
301 the cell, changing their morphology and position, but also that there are different sized
302 chromatin-containing extranuclear bodies within cell cytoplasm. It is important to note
303 that a recent study has demonstrated that chromatin-containing bodies arise from the main
304 nuclei, move within the cell and are ultimately loaded in exosomes (Yokoi et al., 2019).
305 Therefore, it would be interesting to examine whether chromatin-containing bodies can
306 move independently of the movement of the main nuclei or if they are a product of the
307 main nuclei movement.

308 Beyond the central nervous system, the presence of lobed nuclei has been reported in
309 most immune cells, but the functional significance of multilobed nuclear structures is not
310 yet known (Hoffmann et al., 2007; Georgopoulos, 2017; Skinner and Johnson, 2017).
311 What is known is that human leukocytes position their nucleus at the front of the cell
312 during migration (Barzilai et al., 2010). Importantly, the intermediate hBM-MSCs also
313 positioned their nucleus at the front of the cell during migration. Futhermore, binuclear
314 cells are commonly found in various human organs including, heart and liver. The
315 functional significance of these binuclear cells is also not yet known (Guidotti et al., 2003;
316 Miko et al., 2017). The nuclear morphology of hBM-MSCs observed during the

317 transdifferentiation bears a lot of similarities to the nuclear morphology observed in
318 immune cells, hepatocytes and cardiomyocytes. Therefore, it would be interesting to
319 examine whether the nuclear structures observed in these human cells are also associated
320 with nuclear movement within the cell.

321 In the classical view of cell development, progenitor cells differentiate into several
322 distinct cell intermediates, with an increasingly restricted lineage potential, until the final
323 mature, specialised cell types are generated and functionally integrated into their
324 respective tissues. The differentiated state of a cell was believed to be terminal and
325 irreversible (Waddington, 1957). While asymmetric cell division is considered to be the
326 mechanism by which the asymmetric inheritance of cellular components during mitosis
327 defines the distinct fate of each daughter cell (Venkei and Yamashita, 2018). However,
328 there is increasing evidence that these rules can be broken (Blau et al., 200; Rajagopal et
329 al., 2016). It has long been accepted that adult cells can assume new fates without
330 asymmetric cell division through dedifferentiation and transdifferentiation processes, a
331 phenomenon known as cellular plasticity (Raff et al., 2003; Jopling et al., 2011; Merrell
332 et al., 2016;). Current research aims to understand the mechanisms of these these cell
333 conversion processes and eventually harness them for use in regenerative medicine
334 (Jopling et al., 2011; Eguizabal et al., 2013; Slack et al., 2007).

335 In conclusion, our results support the notion that MSCs transdifferentiate towards a neural
336 lineage through a dedifferentiation step followed by re-differentiation to neural
337 phenotypes. Mesenchymal stromal cells MSCs could also help increase our
338 understanding of the mechanisms underlying cellular plasticity and shed light on whether
339 dedifferentiation, transdifferentiation and differentiation occur in different contexts or are
340 different terms for the same cellular process.

341

342

343 # Experimental procedures

344 ## Ethical conduct of research

345 The authors declare that all protocols used to obtain and process all human samples were
346 approved by the local ethics committees (UMH.IN.SM.03.16, HULP3617.05/07/2012
347 and HUSA19/1531.17/02/2020) according to Spanish and European legislation and
348 conformed to the ethical guidelines of the Helsinki Declaration. Donors provided written
349 informed consent before obtaining samples.

350 ## Isolation and culture of hBMSCs

351 Bone marrow aspirates were obtained by percutaneous direct aspiration from the iliac
352 crest of 5 healthy volunteers at University Hospital Virgen de la Arrixaca (Murcia, Spain).
353 Bone marrow was collected with 20 U/ml sodium heparin, followed by a Ficoll density
354 gradient-based separation by centrifugation at 540g for 20 min. After, mononuclear cell
355 fraction was collected, washed twice with Ca^{2+}/Mg^{2+}-free phosphate buffered saline
356 (PBS) (Gibco Invitrogen) and seeded into 175-cm2 culture flasks (Nunc, Thermo Fisher
357 Scientific) at a cell density $1.5x10^5$ cells/cm^2 in serum-containing media (designated as
358 the basal media), composed of DMEM low glucose medium (Thermo Fisher Scientific)
359 supplemented with 10% fetal bovine serum (FBS; Lonza), 1% GlutaMAX (Thermo
360 Fisher Scientific), non-essential amino acid solution (Sigma-Aldrich) and 1%
361 penicillin/streptomycin (Thermo Fisher Scientific). After 3 days of culture at 37ºC and
362 7% CO_2, non-attached cells were removed and fresh complete medium was added.
363 Culture media were renewed every 2 days, and the isolated hBMSCs were passaged when
364 cultures were 70-80% confluent. All studies were performed using hBMSCs expanded
365 within culture passages 3-4.

366

367 **Expression Vectors and Cell Transfection**

368 The expression vectors used in the present study were H2B-eGFP, a gift from Geoff Wahl
369 (Addgene plasmid # 11680; http://n2t.net/addgene:11680; RRID:Addgene_11680;
370 Kanda et al., 1998). Isolated hBMSCs-derived cells were transfected using the Gene
371 Pulser-II Electroporation System (Bio-Rad Laboratories). Electroporation was performed
372 in a sterile cuvette with a 0.4-cm electrode gap (Bio-Rad Laboratories), using a single
373 pulse of 270 V, 500 µF. Plasmid DNA (5 µg) was added to 1.5×10^6 viable hBMSCs-
374 derived cells in 0.2-ml DMEM low glucose medium (Thermo Fisher Scientific) before
375 electrical pulsing.

376 **Time-lapse microscopy of histone H2B-GFP expressing hBM-MSCs cultured in**
377 **neural induction media**

378 We used µ-Dish 35 mm, high Grid- 500 (Ibidi) for live cell imaging. Histone H2B-GFP
379 transfected hBM-MSCs were plated onto collagen IV (Sigma-Aldrich) coated plastic or
380 glass coverslips. To induce neural differentiation, cells at passage 3–4 were allowed to
381 adhere to the plates overnight. Basal media was removed the following day and the cells
382 were cultured for 2 days in serum-free media (designated as the neural basal media)
383 consisting in Dulbecco's modified Eagle's medium/F12 (DMEM/F12 Glutamax, Gibco)
384 supplemented with N2-supplement (R&D systems), 0.6% glucose (Sigma-Aldrich), 5mM
385 HEPES (Sigma-Aldrich), 0.5% human serum albumin (Sigma-Aldrich), 0.0002% heparin
386 (Sigma-Aldrich), non-essential amino acid solution (Sigma-Aldrich) and 100 U/ml
387 penicillin-streptomycin (Sigma-Aldrich). On day 3, cells were cultured in neural
388 induction media, consisting in the neural basal media supplemented with 500nM retinoic
389 acid (Sigma-Aldrich), 1mM dibutyryl cAMP (Sigma-Aldrich) and the growth factors

390 BDNF (10 ng/ml; Peprotech), GDNF (10 ng/ml; Peprotech) and IGF-1 (10 ng/ml; R&D
391 systems). Time-lapse analysis was carried out using a Widefield Leica Thunder-TIRF
392 imager microscope. We perform time-lapse microscopy within the first 71 hr after neural
393 induction media was added directly to the cells. Time-lapse images were obtained every
394 30 min. During imaging, cells were enclosed in a chamber maintained at 37°C under a
395 humidified atmosphere of 5% CO2 in air. Data are representative of ten independent
396 experiments.

397 **Immunocytochemistry**

398 A standard immunocytochemical protocol was used as previously described (Bueno et al.,
399 2013; Bueno et al., 2019; Bueno et al., 2021). Histone H2B-GFP transfected hBM-MSCs
400 were plated onto collagen IV (Sigma-Aldrich) coated plastic or glass coverslips and
401 maintained in neural induction media. Cells were rinsed with PBS and fixed in freshly
402 prepared 4% paraformaldehyde (PFA; Sigma-Aldrich). Fixed cells were blocked for 2 h
403 in PBS containing 10% normal horse serum (Gibco) and 0.25% Triton X-100 (Sigma)
404 and incubated overnight at 4 °C with antibodies against β-III-tubulin (TUJ1; 1:500,
405 Covance) in PBS containing 1% normal horse serum and 0.25% Triton X-100. On the
406 next day, cells were rinsed and incubated with the secondary antibody conjugated with
407 Alexa Fluor® 594 (anti-mouse; 1:500, Molecular Probes). Cell nuclei were
408 counterstained with DAPI (0.2 mg/ml in PBS, Molecular Probes).

409 **Images and Data Analyses**

410 Photograph of visible and fluorescent stained samples were carried out in a Widefield
411 Leica Thunder-TIRF imager microscope equipped with a digital camera or in confocal
412 laser scanning microscope Leica TCS-SP8. We used Filmora Video Editor software for

video editing and Photoshop software to improve the visibility of fluorescence images without altering the underlying data.

Acknowledgements: We greatly appreciate the technical assistance of Microscopy Section and the Tissue Culture Service of the University of Murcia.

Author contributions: C.B. conceived of the study, designed the study, carried out the molecular lab work and drafted the manuscript; M.B. and D.G-B. designed experiments, participated in data analysis and helped draft the manuscript; S.M. and J.M.M. helped draft the manuscript and financial support.

Declaration of interests: The authors declare no competing interests.

Funding: This study was supported by the Spanish Ministry of Science and Innovation, the Carlos III Health Institute (ISCIII), through the Spanish Network of Cell Therapy (TerCel), RETICS subprogram, projects RD16/0011/0001 and RD16/0011/0010, co-funded by European Regional Development Fund (ERDF) "Una manera de hacer Europa". It was also partially supported by MINECO/AEI/ERDF, EU, Spanish Ministry of Economy, Industry and Competitiveness, the Spanish State Research Agency and the European Union through the ERDF– "Una manera de hacer Europa" (proyect SAF2017-83702-R); The Generalitat Valenciana (Prometeo/2018/041); Research Grant of the Universidad Católica San Antonio de Murcia (UCAM).

435

436

437

438 ## References

439 Alvarez-Dolado, M., Pardal, R., Garcia-Verdugo, J.M., Fike, J.R., Lee, H.O., Pfeffer, K.,
440 Lois, C., Morrison, S.J., and Alvarez-Buylla, A. (2003). Fusion of bone-marrow-derived
441 cells with Purkinje neurons, cardiomyocytes and hepatocytes. Nature *425*, 968-973.
442 10.1038/nature02069.

443 Altman, J. (1963). Autoradiographic investigation of cell proliferation in the brains of rats
444 and cats. Anat. Rec. *145*, 573-591. 10.1002/ar.1091450409.

445 Azedi, F., Kazemnejad, S., Zarnani, A.H., Soleimani, M., Shojaei, A., and Arasteh, S.
446 (2017). Comparative capability of menstrual blood versus bone marrow derived stem
447 cells in neural differentiation. Mol. Biol. Rep. *44*, 169–182. 10.1007/s11033-016-4095-
448 7.

449 Azizi, A.S., Stokes, D., Augelli, B.J., DiGirolamo, C., and Prockop, D.J. (1998).
450 Engraftment and migration of human bone marrow stromal cells implanted in the brains
451 of albino rats – similarities to astrocyte grafts. Proc. Natl. Acad. Sci. U S A *95*, 3908-
452 3913. 10.1073/pnas.95.7.3908.

453 Barzilai, S., Yadav, S.K., Morrell, S., Roncato, F., Klein, E., Stoler-Barak, L., Golani, O.,
454 Feigelson, S.W., Zemel, A., Nourshargh, S., et al. (2017). Leukocytes Breach Endothelial
455 Barriers by Insertion of Nuclear Lobes and Disassembly of Endothelial Actin Filaments.
456 Cell Rep. *18*, 685-699. 10.1016/j.celrep.2016.12.076.

457 Bertani, N., Malatesta, P., Volpi, G., Sonego, P., and Perris. R. (2005). Neurogenic
458 potential of human mesenchymal stem cells revisited: analysis by immunostaining, time-
459 lapse video and microarray. J. Cell Sci. *118*, 3925-3936. 10.1242/jcs.02511.

460 Blau, H.M., Brazelton, T.H., and Weimann, J.M. (2001). The evolving concept of a stem
461 cell: entity or function? Cell *105*, 829-841. 10.1016/s0092-8674(01)00409-3.

462 Bond, A. M., Ming, G.L., and Song, H. (2015). Adult mammalian neural stem cells and
463 neurogenesis: five decades later. Cell Stem Cell *17*, 385–395.
464 10.1016/j.stem.2015.09.003.

465 Brazelton, T.R., Rossi, F.M, Keshet, G.I.,and Blau, H.M. (2000). From marrow to brain:
466 expression of neuronal phenotypes in adult mice. Science. *290*, 1775-1779.
467 10.1126/science.290.5497.1775.

468 Breunig, J.J., Arellano, J.I., Macklis, J.D., and Rakic, P. (2007). Everything that glitters
469 isn't gold: a critical review of postnatal neural precursor analyses. Cell Stem Cell. *1*, 612–
470 627. 10.1016/j.stem.2007.11.008.

471 Bueno, C., Ramirez, C., Rodríguez-Lozano, F.J, Tabarés-Seisdedos, R., Rodenas, M.,
472 Moraleda, J.M., Jones, J.R., and Martinez, S. (2013). Human adult periodontal ligament-
473 derived cells integrate and differentiate after implantation into the adult mammalian brain.
474 Cell Transplant. *22*, 2017–2028. 10.3727/096368912X657305.

475 Bueno, C., Martínez-Morga, M., and Martínez, S. (2019). Non-proliferative neurogenesis
476 in human periodontal ligament stem cells. Sci. Rep. *9*, 18038. 101038/s41598-019-
477 54745-3.

478 Bueno, C., Martínez-Morga, M., García-Bernal, D., Moraleda, J.M., and Martínez, S.
479 (2021). Differentiation of human adult-derived stem cells towards a neural lineage

480 involves a dedifferentiation event prior to differentiation to neural phenotypes. Sci Rep.
481 *11*, 12034. 10.1038/s41598-021-91566-9.

482 Capilla-Gonzalez, V., Cebrian-Silla, A., Guerrero-Cazares, H., Garcia-Verdugo, J.M. and
483 Quiñones-Hinojosa, A. (2014). Age-related changes in astrocytic and ependymal cells of
484 the subventricular zone. Glia *62*, 790–803. 10.1002/glia.22642.

485 Cebrián-Silla, A., Alfaro-Cervelló, C., Herranz-Pérez, V., Kaneko, N., Park, D.H,
486 Sawamoto, K., Alvarez-Buylla, A., Lim, D.A., and García-Verdugo, J.M. (2017). Unique
487 organization of the nuclear envelope in the post-natal quiescent neural stem cells. Stem
488 Cell Reports *9*, 203–216. 10.1016/j.stemcr.2017.05.024.

489 Cooper-Kuhn, C.M., and Kuhn, H.G. Is it all DNA repair? (2002). Methodological
490 considerations for detecting neurogenesis in the adult brain. Brain Res. Dev *134*, 13–21.
491 0.1016/s0165-3806(01)00243-7.

492 Das, G.D. (1977). Binucleated neurons in the central nervous system of the laboratory
493 animals. Experientia *33*, 1179-80. 10.1007/BF01922313.

494 Doetsch, F., Garcia-verdugo, J.M., and Alvarez-buylla, A. (1997). Cellular composition
495 and three-dimensional organization of the subventricular germinal zone in the adult
496 mammalian brain. J. Neurosci. *17*, 5046–5061. 10.1523/JNEUROSCI.17-13-
497 05046.1997.

498 Doetsch, F., Garcia-verdugo, J.M., and Alvarez-buylla, A. (1999a). Regeneration of a
499 germinal layer in the adult mammalian brain. Proc. Natl. Acad. Sci. *96*, 11619–11624.
500 10.1073/pnas.96.20.11619.

501 Doetsch, F., Caillé, I., Garcia-verdugo, J.M.,and Alvarez-buylla, A. (1999b).
502 Subventricular zone astrocytes are neural stem cells in the adult mammalian brain. Cell.
503 *97*, 703–716. 10.1016/S0092-8674(00)80783-7.

504 Eguizabal, C., Montserrat, N., Veiga, A., and Izpisua Belmonte J.C. (2013).
505 Dedifferentiation, transdifferentiation, and reprogramming: future directions in
506 regenerative medicine. Semin. Reprod. Med. *31*, 82-94. 10.1055/s-0032-1331802.

507 Filippov, V., Kronenberg, G., Pivneva, T., Reuter, K., Steiner, B, Wang, L.P.,
508 Yamaguchi, M., Kettenmann, H., and Kempermann, G. (2003). Subpopulation of nestin-
509 expressing progenitor cells in the adult murine hippocampus shows electrophysiological
510 and morphological characteristics of astrocytes. Mol. Cell Neurosci. *23*, 373-382.
511 10.1016/s1044-7431(03)00060-5.

512 Guidotti, J.E., Brégerie, O., Robert, A., Debey, P., Brechot, C., and Desdouets C. (2003).
513 Liver cell polyploidization: a pivotal role for binuclear hepatocytes. J. Biol. Chem. *278*,
514 19095-19101. 10.1074/jbc.M300982200.

515 Georgopoulos, K. (2017). In search of the mechanism that shapes the neutrophil´s
516 nucleus. Genes Dev. *31*, 85–87. 10.1101/gad.296228.117.

517 Guerrero-Cázares, H., Gonzalez-Perez, O., Soriano-Navarro, M., Zamora-Berridi, G.,
518 García-Verdugo, J.M., and Quinoñes-Hinojosa, A. (2011). Cytoarchitecture of the lateral
519 ganglionic eminence and rostral extension of the lateral ventricle in the human fetal brain.
520 J. Comp. Neurol. *519*, 1165–1180. 10.1002/cne.22566.

521 Grove, J.E., Bruscia, E., and Krause, D.S. (2004). Plasticity of bone marrow-derived stem
522 cells. Stem Cells. *22*, 487-500. 10.1634/stemcells.22-4-487.

523 Hermann, A., Liebau, S., Gast,l R., Fickert, S., Habisch, H.J., Fiedler, J., Schwarz, J.,
524 Brenner, R., and Storch, A. (2006). Comparative analysis of neuroectodermal
525 differentiation capacity of human bone marrow stromal cells using various conversion
526 protocols. J. Neurosci. Res. *83*, 1502-1514. 10.1002/jnr.20840.

527 Hernández, R., Jiménez-Luna, C., Perales-Adán, J., Perazzoli, G., Melguizo, C., and
528 Prados, J. (2020). Differentiation of Human Mesenchymal Stem Cells towards Neuronal
529 Lineage: Clinical Trials in Nervous System Disorders. Biomol Ther (Seoul). *28*, 34-44.
530 10.4062/biomolther.2019.065.

531 Hoffmann, K., Sperling, K., Olins, A.L., and Olins, D.E. (2007). The granulocyte nucleus
532 and lamin B receptor: avoiding the ovoid. Chromosoma. *116*, 227-235. 10.1007/s00412-
533 007-0094-8.

534 Jeong, J.A., Gang, E.J., Hong, S.H., Hwang, S.H., Kim, S.W., Yang, I.H., Ahn, C.,
535 Han,H., and Kim, H. (2004). Rapid neural differentiation of human cord blood-derived
536 mesenchymal stem cells. Neuroreport *15*, 1731–1734.
537 10.1097/01.wnr.0000134846.79002.5c.

538 Jopling, C., Boue, S., and Izpisua Belmonte J.C. (2011). Dedifferentiation,
539 transdifferentiation and reprogramming: three routes to regeneration. Nat. Rev. Mol. Cell
540 Biol. *12*, 79-89. 10.1038/nrm3043.

541 Kanda, T., Sullivan, K.F., and Wahl, G.M. (1998). Histone-GFP fusion protein enables
542 sensitive analysis of chromosome dynamics in living mammalian cells. Curr. Biol. *8*, 377-
543 385. 10.1016/s0960-9822(98)70156-3.

544 Kemp, K., Wilkins, A., and Scolding, N. (2014). Cell fusion in the brain: two cells
545 forward, one cell back. Acta Neuropathol. *128*, 629-38. 10.1007/s00401-014-1303-1.

546 Kempermann, G., Jessberger, S., Steiner, B., and Kronenberg, G. (2004). Milestones of
547 neuronal development in the adult hippocampus. Trends. Neurosci. *27*, 447–452.
548 10.1016/j.tins.2004.05.013.

549 Kopen, G.C., Prockop, D.J., and Phinney, D.G. (1999). Marrow stromal cells migrate
550 throughout forebrain and cerebellum, and they differentiate into astrocytes after injection
551 into neonatal mouse brains. Proc. Natl. Acad. Sci. USA *96*, 10711–10716.
552 10.1073/pnas.96.19.10711.

553 Krabbe. C, Zimmer. J., and Meyer, M. (2005). Neural transdifferentiation of
554 mesenchymal stem cells—A critical review. APMIS. *113*, 831–844. 10.1111/j.1600-
555 0463.2005.apm_3061.x

556 Kronenberg, G., Reuter, K., Steiner, B., Brandt, M.D., Jessberger, S., Yamaguchi, M.,
557 and Kempermann, G. (2003). Subpopulations of proliferating cells of the adult
558 hippocampus respond differently to physiologic neurogenic stimuli. J. Comp. Neurol.
559 *467*, 455-463. 10.1002/cne.10945.

560 Kuhn, H.G., Eisch, A.J., Spalding, K., and Peterson, D.A. (2016). Detection and
561 Phenotypic Characterization of Adult. Neurogenesis. Cold Spring Harb. Perspect. Biol.
562 *8*, a025981. 10.1101/cshperspect.a025981.

563 Lu, P., Blesch, A., and Tuszynski, M.H. (2004). Induction of bone marrow stromal cells
564 to neurons: differentiation, transdifferentiation, or artifact? J. Neurosci. Res. *77*, 174-191.
565 10.1002/jnr.20148.

566 Magrassi, L., Grimaldi, P., Ibatici A., Corselli, M., Ciardelli, L., Castello, S., Podestà, M.,
567 Frassoni, F., and Rossi, F. (2007). Induction and survival of binucleated Purkinje neurons
568 by selective damage and aging. J. Neurosci. *27*, 9885-9892. 10.1523/JNEUROSCI.2539-
569 07.2007.

570 Merrell, A.J., and Stanger, B.Z. (2016). Adult cell plasticity in vivo: de-differentiation
571 and transdifferentiation are back in style. Nat. Rev. Mol. Cell Biol. *17*, 413-25.
572 10.1038/nrm.2016.24.

573 Mezey, E., Chandross, K.J., Harta, G., Maki, R.A., and McKercher, S.R. (2000). Turning
574 blood into brain: cells bearing neuronal antigens generated in vivo from bone marrow.
575 Science. *290*, 1779-82. 10.1126/science.290.5497.1779.

576 Mezey E., Key, S., Vogelsang, G., Szalayova, I., Lange, G.D., and Crain, B. (2003).
577 Transplanted bone marrow generates new neurons in human brains. Proc. Natl. Acad. Sci.
578 U S A. *100*,1364-1369. 10.1073/pnas.0336479100.

579 Miko, M., Kyselovic, J., Danisovic, L., Barczi, T., Polak, S., and Varga, I. (2017). Two
580 nuclei inside a single cardiac muscle cell. More questions than answers about the
581 binucleation of cardiomyocytes. Biologia *72*, 825–830. 10.1515/biolog-2017-0107.

582 Monje, P.V., Soto, J., Bacallao, K., and Wood, P.M. (2010). Schwann cell
583 dedifferentiation is independent of mitogenic signaling and uncoupled to proliferation:
584 role of cAMP and JNK in the maintenance of the differentiated state. J. Biol. Chem. *285*,
585 31024-31036. 10.1074/jbc.M110.116970.

586 Muñoz-Elias, G., Marcus, A.J., Coyne, T.M., Woodbury, D., and Black, I.B. (2004).
587 Adult bone marrow stromal cells in the embryonic brain: engraftment, migration,
588 differentiation, differentiation, and long-term survival. J. Neurosci. *24*, 4585-4595.
589 10.1523/JNEUROSCI.5060-03.2004.

590 Muñoz-Elias, G., Woodbury, D., and Black, I.B. (2003). Marrow stromal cells, mitosis
591 and neuronal differentiation: stem cell and precursor functions. Stem Cells *21*,437–448.
592 10.1634/stemcells.21-4-437.

593 Nern, C., Wolff, I., Macas, J., von Randow, J., Scharenberg, C., Priller, J., and Momma,
594 S. (2009) Fusion of hematopoietic cells with Purkinje neurons does not lead to stable
595 heterokaryon formation under noninvasive conditions. J. Neurosci. *29*, 3799-807.
596 10.1523/JNEUROSCI.5848-08.2009.

597 Neuhuber, B., Gallo, G., Howard, L., Kostura, L., Mackay, A., and Fischer, I. (2004).
598 Reevaluation of in vitro differentiation protocols for bone marrow stromal cells:
599 disruption of actin cytoskeleton induces rapid morphological changes and mimics
600 neuronal phenotype. J. Neurosci. Res. *77*, 192-204. 10.1002/jnr.20147.

601 Ning, H., Lin, G., Lue, T.F., and Lin, C.S. (2006). Neuron-like differentiation of adipose
602 tissue-derived stromal cells and vascular smooth muscle cells. Differentiation *74*, 510-
603 518. 10.1111/j.1432-0436.2006.00081.x.

604 Phinney, D.G, and Prockop, D.J. (2007) Concise review: mesenchymal stem/multipotent
605 stromal cells: the state of transdifferentiation and modes of tissue repair--current views.
606 Stem Cells *25*, 2896-28902. 10.1634/stemcells.2007-0637.

607 Portiansky, E.L., Barbeito, C.G., Flamini, M.A., Gimeno, E.J., and Goya, R.G. (2006)
608 Presence of binucleate neurons in the spinal cord of young and senile rats. Acta
609 Neuropathol. *112*, 647-649. 10.1007/s00401-006-0139-8

610 Priller, J., Persons, D.A., Klett, F.F., Kempermann, G., Kreutzberg, G.W., and Dirnagl,
611 U. (2001). Neogenesis of cerebellar Purkinje neurons from gene-marked bone marrow
612 cells in vivo. J. Cell Biol. *155*, 733-738. 10.1083/jcb.200105103.

613 Radhakrishnan, S., Trentz, O.A., Reddy, M.S., Rela, M., Kandasamy, M., and
614 Sellathamby, S. (2019). In vitro transdifferentiation of human adipose tissue-derived stem
615 cells to neural lineage cells - a stage-specific incidence. Adipocyte *8*, 164–177.
616 10.1080/21623945.2019.1607424.

617 Raff, M. Adult stem cell plasticity: fact or artifact? (2003). Annu. Rev. Cell Dev. Biol.
618 *19*, 1-22. 10.1146/annurev.cellbio.19.111301.143037.

619 Rajagopal, J., and Stanger B.Z. (2016). Plasticity in the Adult: How Should the
620 Waddington Diagram Be Applied to Regenerating Tissues? Dev. Cell *36*, 133-137.
621 10.1016/j.devcel.2015.12.021.

622 Rakic, P. (2002). Adult neurogenesis in mammals: an identity crisis. J. Neurosci. *22*, 614–
623 618. 10.1523/JNEUROSCI.22-03-00614.2002.

624 Ribak, C.E, and Seress, L. (1983). Five types of basket cell in the hippocampal dentate
625 gyrus: a combined Golgi and electron microscopic study. J. Neurocytol. *12*, 577-597.
626 10.1007/BF01181525

627 Seri, B., Garcia-verdugo, J.M., McEwen, B.S, and Alvarez-buylla, A. (2001). Astrocytes
628 give rise to new neurons in the adult mammalian hippocampus. J. Neurosci. *21*,7153–
629 7160. 10.1523/JNEUROSCI.21-18-07153.2001.

630 Seri, B., Garcia-verdugo, J.M., Collado-Morente, L., McEwen, B.S., and Alvarez-buylla,
631 A. (2004). Cell types, lineage, and architecture of the germinal zone in the adult dentate
632 gyrus. J. Comp. Neurol. *474*, 359–378. 10.1002/cne.20288.

633 Slack, J.M. (2007). Metaplasia and transdifferentiation: from pure biology to the clinic.
634 Nat Rev Mol. Cell Biol. *8*, 369-78. 10.1038/nrm2146.

635 Skinner, B.M., and Johnson, E.E. (2017). Nuclear morphologies: their diversity and
636 functional relevance. Chromosoma. *126*, 195–212. 10.1007/s00412-016-0614-5

637 Sorrells, S.F., Paredes, M.F., Zhang, Z., Kang, G., Pastor-Alonso, O., Biagiotti, S., Page,
638 C.E., Sandoval, K., Knox, A., Connolly, A., et al. (2021). Positive controls in adults and

639 children support that very few, if any, new neurons are born in the adult human
640 hippocampus. J. Neurosci. *41*, 2554–2565. 10.1523/JNEUROSCI.0676-20.2020.

641 Suon, S., Jin, H., Donaldson, A.E., Caterson, E.J., Tuan, R.S., Deschennes, G., Marshall,
642 C., and Iacovitti, L. (2004). Transient differentiation of adult human bone marrow cells
643 into neuron-like cells in culture: development of morphological and biochemical traits is
644 mediated by different molecular mechanisms. Stem Cells Dev. *13*, 625-635.
645 10.1089/scd.2004.13.625.

646 Venkei, G.Z., and Yamashita, Y.M. (2018). Emerging mechanisms of asymmetric stem
647 cell division. J. Cell Biol. *217*, 3785–3795. 10.1083/jcb.201807037.

648 Waddington, C. H. (1957). The Strategy of the Genes. A Discussion of Some Aspects of
649 Theoretical Biology. Crows Nest: Allen & Unwin.

650 Weimann, J.M., Johansson, C.B., Trejo, A., and Blau, H.M. (2003). Stable reprogrammed
651 heterokaryons form spontaneously in Purkinje neurons after bone marrow transplant. Nat.
652 Cell Biol. 5, 959-966. 10.1038/ncb1053.

653 Wittmann, M., Queisser, G., Eder, A., Wiegert, J.S., Bengtson, C.P., Hellwig, A., Wittum,
654 G., and Bading, H. (2009). Synaptic activity induces dramatic changes in the geometry
655 of the cell nucleus: interplay between nuclear structure, histone H3 phosphorylation, and
656 nuclear calcium signaling. J. Neurosci. *29*, 14687–14700. 10.1523/JNEUROSCI.1160-
657 09.2009.

658 Woodbury, D., Schwarz, E.J., Prockop, D.J, and Black IB. (2000). Adult rat and human
659 bone marrow stromal stem cells differentiate into neurons. J. Neurosci. Res. *61*, 364-370.
660 10.1002/1097-4547(20000815)61:4<364::AID-JNR2>3.0.CO;2-C.

661 Woodbury, D., Reynolds, K., and Black, I.B. (2002). Adult bone marrow stromal stem
662 cells express germline, ectodermal, endodermal, and mesodermal genes prior to
663 neurogenesis. J. Neurosci. Res *69*, 908-917. 10.1002/jnr.10365.

664 Yokoi A, et al. (2019). Mechanisms of nuclear content loading to exosomes. Sci. Adv.
665 5:eaax8849. 10.1126/sciadvaax8849.

666

667 ## Figure legends

668 **Figure 1. Morphological changes in hBM-MSC cultures during neural**
669 **transdifferentiation**. Time-lapse imaging revealed that, following neural induction,
670 hBM-MSCs rapidly reshaped from a flat to a spherical morphology. Subsequently, we
671 observed that hBM-MSC-derived round cells can preserve their spherical shape for
672 several days (green arrows), change to that of neural-like cells through active neurite
673 extension (red arrows) or revert back to the mesenchymal morphology (yellow arrows).
674 Scale bar: 25 μm.

675 **Figure 2. Morphological changes in dedifferentiated hBM-MSC.** Time-lapse imaging
676 showed the appearance (arrows), movement and disappearance (asterisk) of cellular
677 protrusión from the surface of hBM-MSC-derived round cells. Scale bar: 25 μm.

678 **Figure 3. Neuronal polarisation of dedifferentiated hBM-MSCs.** Time-lapse imaging
679 revealed the growth of new neurites from the body of round cells that which gradually
680 adopted a complex morphology, acquiring dendrite-like (green arrows) and axon-like
681 domains (yellow arrows). There was no observation of any transient cellular protrusión
682 as hBM-MSC-derived round cells gradually acquired a neural-like morphology. Scale
683 bar: 25 μm.

684 **Figure 4. hBMSCs can repeatedly switch lineages.** Time-lapse imaging showed that
685 hBM-MSCs can also rapidly switch lineages without cell division. Mesenchymal
686 morphology (green arrows); switching lineages (white arrows); dediffentiation
687 morphology (red arrows); neural-like morphology (yellow arrows). Scale bar: 25 μm.

688 **Figure 5. Nucleus remodelling occurs during neural transdifferentiation from hBM-**
689 **MSCs.** Time-lapse microscopy evidenced that nuclear remodelling occurred during
690 neural transdifferentiation from histone H2B-GFP-expressing hBM-MSCs. Nuclei from
691 hBM-MSC-derived round cells moved within the cell, adopting different morphologies,
692 including finger shaped (red arrows) and kidney shaped (white arrows), and even forming
693 lobed nuclei connected by nucleoplasmic bridges (yellow arrows). Scale bar: 25 μm.

694 **Figure 6. Nuclear movement generated cellular protrusions that appeared and**
695 **disappeared from the surface of hBM-MSC-derived round cells.** Time-lapse
696 microscopy revealed that the cell nucleus of histone H2B-GFP-expressing hBM-MSCs
697 acquired a finger-like shape and moved within the cell, generating the transient cellular
698 protrusions (arrows) on the surface of the hBM-MSC-derived round cells. Scale bar: 25
699 μm. PhC: Phase-contrast photomicrographs.

700 **Figure 7. Intermediate hBM-MSC nuclei can switch their morphology and**
701 **positioning.** Time-lapse microscopy highlighted that the cell nucleus from histone H2B-
702 GFP-expressing hBM-MSCs can switch its morphology while it is moving. Here, the
703 nucleus acquired a finger-like shape before reorienting toward a peripheral position
704 within the cell and acquiring a kidney-like shape. Subsequently, the cell nucleus began to
705 move rapidly around the cell. Scale bar: 25 μm.

706 **Figure 8. Binucleated hBM-MSCs can form with independence of any cell fusion**
707 **events.** Time-lapse microscopy revealed that the nuclei from histone H2B-GFP-

708 expressing, dedifferentiated hBM-MSCs can move within the cell, forming lobed nuclei
709 connected by nucleoplasmic bridges. The movement of the lobed nuclei also generated
710 cellular transient protrusions from the surface of hBM-MSC-derived round cells. Scale
711 bar: 25 μm. PhC: Phase-contrast photomicrographs.

712 **Figure 9. Mononucleated intermediate hBM-MSCs position their nucleus at the**
713 **front of the cell during migration. A)** Time-lapse microscopy showed that kidney-
714 shaped, histone H2B-GFP-expressing, intermediate hBM-MSCs cells positioned their
715 nucleus at the front of the cell during migration. **B)** In addition, finger-shaped, histone
716 H2B-GFP-expressing, intermediate hBM-MSCs also positioned their nuclei at the front
717 of the cell during migration. Scale bar: 25 μm.

718 **Figure 10. Intermediate hBM-MSC with lobed nuclei position their nucleus at the**
719 **front of the cell during migration. A)** Time-lapse microscopy showed that histone H2B-
720 GFP-expressing, intermediate hBM-MSCs with lobed nuclei positioned their nucleus at
721 the front of the cell during migration. **B)** Futhermore, histone H2B-GFP- expressing,
722 intermediate hBM-MSCs with lobed nuclei positioned their largest lobe at the front of the
723 cell during migration. Scale bar: 25 μm.

724 **Figure 11. Nuclear morphology and positioning during neuronal polarisation of**
725 **intermediate hBM-MSCs.** Time-lapse microscopy did not reveal any changes in nuclear
726 positioning or lobed nuclei formation as histone H2B-GFP-expressing, hBM-MSC-
727 derived round cells gradually acquired a neural-like morphology (asterisks). Scale bar: 25
728 μm.

729 **Figure 12. Nuclear morphology when hBM-MSC-derived round cells redifferentiate**
730 **back to the mesenchymal fate. A)** Time-lapse microscopy revealed that when histone
731 H2B-GFP-expressing, dedifferentiated hBM-MSCs with a single nucleus reverted back

732 to the mesenchymal morphology (asterisk), the nuclei gradually reverted back to their
733 original ellipsoid shape. **B)** By contrast, when histone H2B-GFP-expressing,
734 dedifferentiated hBM-MSCs with lobed nuclei reverted back to the mesenchymal
735 morphology (asterisk), the lobed nuclei were maintained for hours. Scale bar: 25 μm.

736 **Figure 13. hBM-MSCs exhibit unusual nuclear structures and chromatin-**
737 **containing bodies in the cellular cytoplasm during neural transdifferentiation. A)**
738 Confocal microscopy analysis showed that histone H2B-GFP-expressing hBM-MSCs
739 with a finger-shaped nucleus can also present chromatin-containing bodies in the cellular
740 cytoplasm. **B)** Histone H2B-GFP-expressing hBM-MSCs a kidney-shaped nucleus can
741 also exhibit chromatin-containing bodies in the cellular cytoplasm. **C)** Histone H2B-GFP-
742 expressing hBM-MSCs with a lobed nucleus connected by nucleoplasmic bridges can
743 also exhibit chromatin-containing bodies in the cellular cytoplasm. **D)** We noted that
744 histone H2B-GFP-expressing hBM-MSCs with chromatin-containing bodies were
745 connected to the main body of the nucleus by thin strands of nuclear material. **E)**
746 Furthermore, histone H2B-GFP-expressing hBM-MSCs with chromatin-containing
747 bodies moved away from or toward the main nuclei. **F)** Histone H2B-GFP-expressing
748 hBM-MSCs with two lobed nuclei unconnected by any nucleoplasmic bridges with
749 chromatin-containing bodies in the cellular cytoplasmwere also observed. Scale bar: 10
750 μm.

751

752 ## Video legends

753 **Video 1.** Time-lapse imaging revealed that, following neural induction, hBM-MSCs
754 rapidly reshaped from a flat to a spherical morphology. Subsequently, we observed that
755 hBM-MSC-derived round cells can preserve their spherical shape for several days,

756 change to that of neural-like cells through active neurite extension or revert back to the
757 mesenchymal morphology. Related to Figure 1.

758 **Video 2.** Time-lapse imaging showed the appearance, movement and disappearance of
759 cellular protrusión from the surface of hBM-MSC-derived round cells. Related to Figure
760 2.

761 **Video 3.** Time-lapse imaging revealed the growth of new neurites from the body of round
762 cells that which gradually adopted a complex morphology, acquiring dendrite-like and
763 axon-like domains. There was no observation of any transient cellular protrusión as hBM-
764 MSC-derived round cells gradually acquired a neural-like morphology. Related to Figure
765 3.

766 **Video 4.** Time-lapse imaging showed that hBM-MSCs can also rapidly switch lineages
767 without cell division. Related to Figure 4.

768 **Video 5.** Time-lapse microscopy evidenced that nuclear remodelling occurred during
769 neural transdifferentiation from histone H2B-GFP-expressing hBM-MSCs. Nuclei from
770 hBM-MSC-derived round cells moved within the cell, adopting different morphologies,
771 including finger shaped and kidney shaped, and even forming lobed nuclei connected by
772 nucleoplasmic bridges. Related to Figure 5.

773 **Video 6.** Time-lapse microscopy revealed that the cell nucleus of histone H2B-GFP-
774 expressing hBM-MSCs acquired a finger-like shape and moved within the cell,
775 generating the transient cellular protrusions on the surface of the hBM-MSC-derived
776 round cells. Related to Figure 6.

777 **Video 7.** Time-lapse microscopy highlighted that the cell nucleus from histone H2B-
778 GFP-expressing hBM-MSCs can switch its morphology while it is moving. Here, the
779 nucleus acquired a finger-like shape before reorienting toward a peripheral position

780 within the cell and acquiring a kidney-like shape. Subsequently, the cell nucleus began to
781 move rapidly around the cell. Related to Figure S1.

782 **Video 8.** Time-lapse microscopy revealed that the nuclei from histone H2B-GFP-
783 expressing, dedifferentiated hBM-MSCs can move within the cell, forming lobed nuclei
784 connected by nucleoplasmic bridges. The movement of the lobed nuclei also generated
785 cellular transient protrusions from the surface of hBM-MSC-derived round cells. Related
786 to Figure 7.

787 **Video 9.** Time-lapse microscopy showed that kidney-shaped, histone H2B-GFP-
788 expressing, dedifferentiated hBM-MSCs cells positioned their nucleus at the front of the
789 cell during migration. Related to Figure S2A.

790 **Video 10.** Time-lapse microscopy showed that finger-shaped histone H2B-GFP-
791 expressing, dedifferentiated hBM-MSCs also positioned their nuclei at the front of the
792 cell during migration. Related to Figure S2B.

793 **Video 11.** Time-lapse microscopy showed that histone H2B-GFP-expressing,
794 dedifferentiated hBM-MSCs with lobed nuclei positioned their nucleus at the front of the
795 cell during migration. Related to Figure S3A.

796 **Video 12.** Time-lapse microscopy showed that histone H2B-GFP-expressing,
797 dedifferentiated hBM-MSCs with lobed nuclei positioned their largest lobe at the front of
798 the cell during migration. Related to Figure S3B.

799 **Video 13.** Time-lapse microscopy did not reveal any changes in nuclear positioning or
800 lobed nuclei formation as histone H2B-GFP-expressing, hBM-MSC-derived round cells
801 gradually acquired a neural-like morphology. Related to Figure S4.

802 **Video 14.** Time-lapse microscopy revealed that when histone H2B-GFP-expressing,
803 dedifferentiated hBM-MSCs with a single nucleus reverted back to the mesenchymal
804 morphology, the nuclei gradually reverted back to their original ellipsoid shape. Related
805 to Figure S5A.

806 **Video 15.** Time-lapse microscopy revealed that when histone H2B-GFP-expressing,
807 dedifferentiated hBM-MSCs with lobed nuclei reverted back to the mesenchymal
808 morphology, the lobed nuclei were maintained for hours. Related to Figure S5B.

809

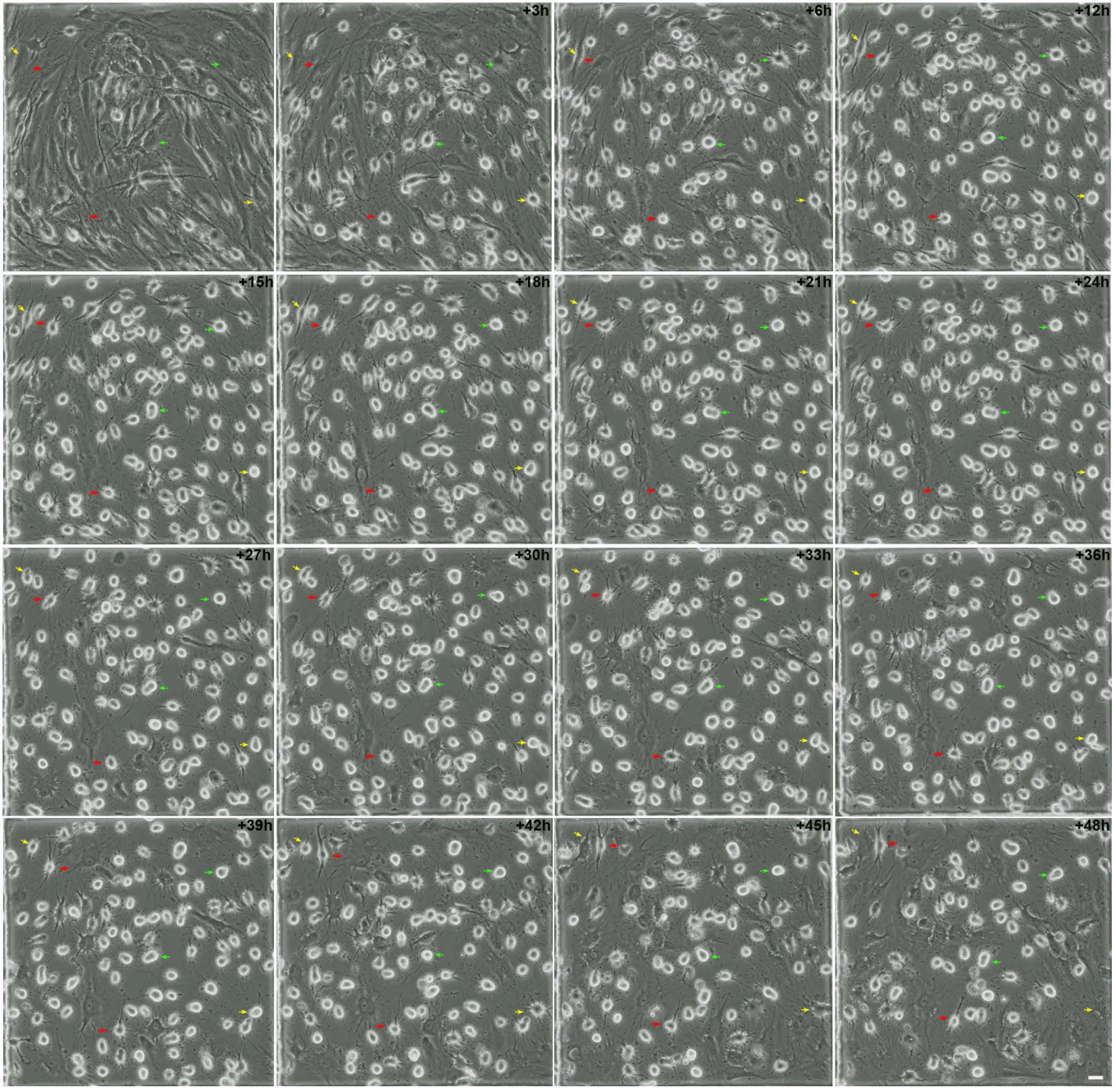

Figure 1

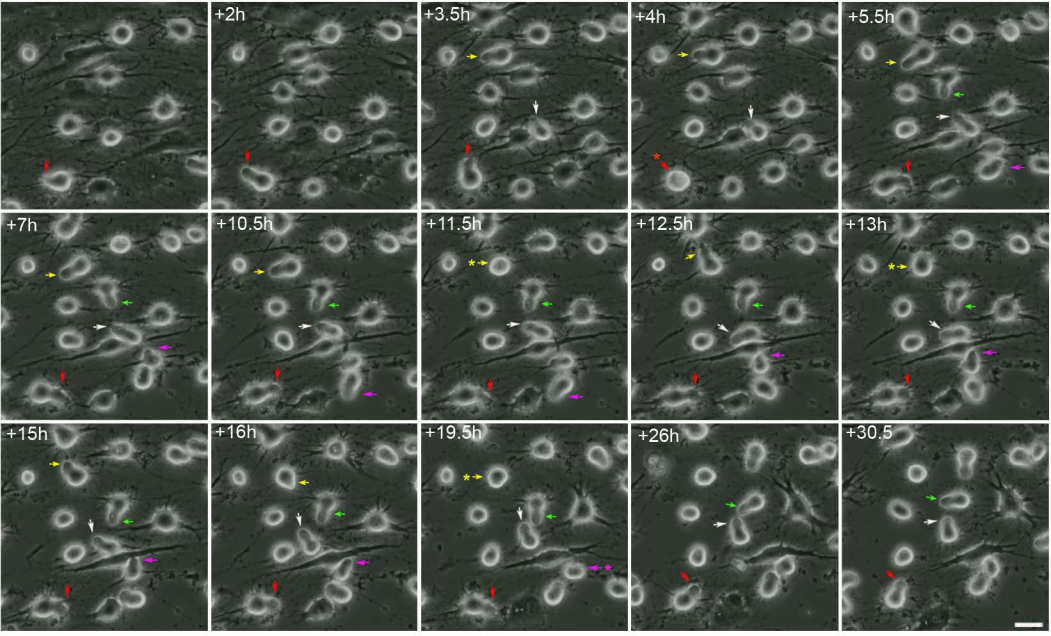

Figure 2

+0.5h
+1h
+1.5h
+2h
+2.5h
+3h
+3.5h
+4h
+4.5h
+5h
+5.5h
+6h
+6.5h
+7h
+7.5h
+8h
+8.5h
+9h
+9.5h
+10h
+10.5h
+11h
+11.5h
+12h
+12.5h
+13h
+13.5h
+14h
+14.5h
+15h
+15.5h
+16h
+16.5h
+17h
+17.5h
+18h
+18.5h
+19h
+19.5h
+20h
+20.5h
+21h
+21.5h
+22h
+22.5h
+23.5h
+24h
+24.5h

Figure 3

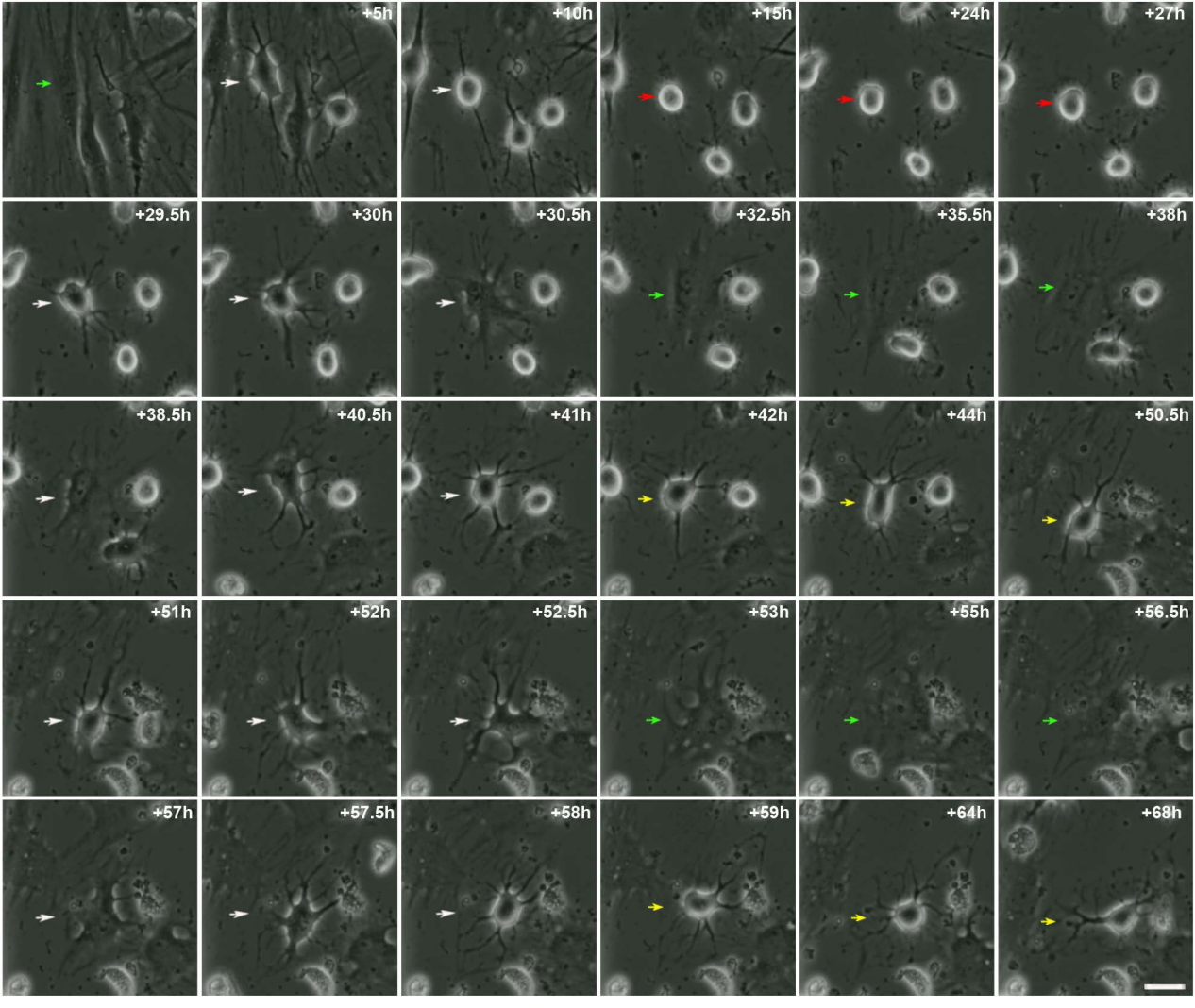
+5h
+10h
+15h
+24h
+27h
+29.5h
+30h
+30.5h
+32.5h
+35.5h
+38h
+38.5h
+40.5h
+41h
+42h
+44h
+50.5h
+51h
+52h
+52.5h
+53h
+55h
+56.5h
+57h
+57.5h
+58h
+59h
+64h
+68h

Figure 4

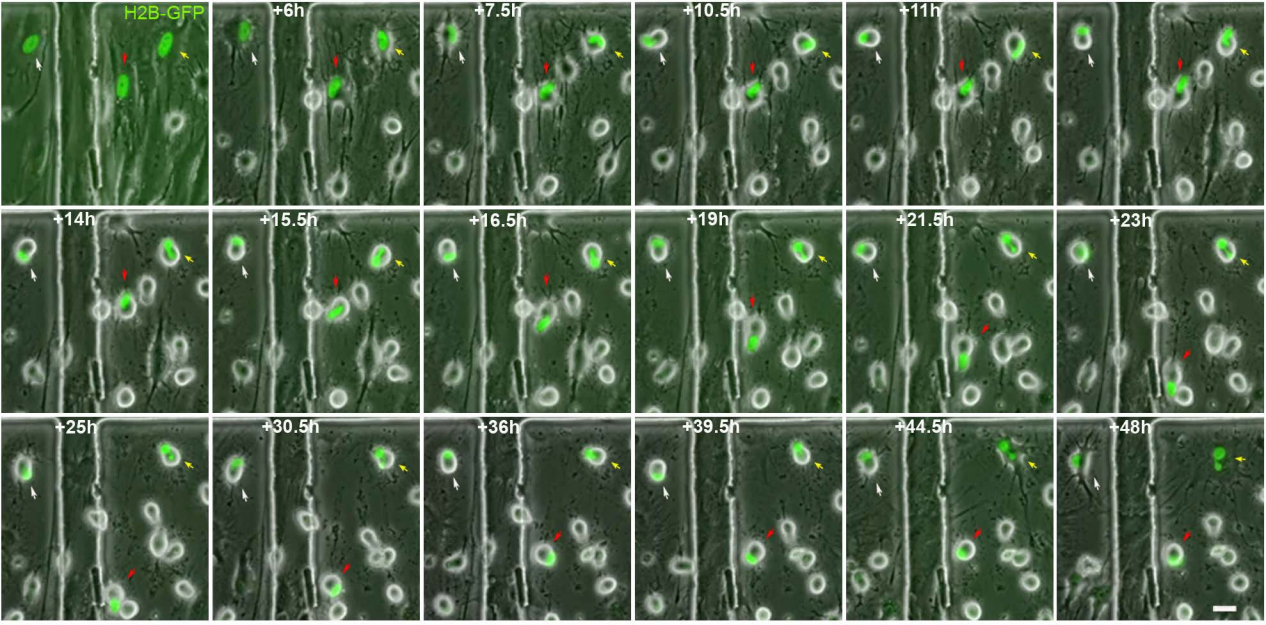
H2B-GFP
+6h
+7.5h
+10.5h
+11h
+14h
+15.5h
+16.5h
+19h
+21.5h
+23h
+25h
+30.5h
+36h
+39.5h
+44.5h
+48h

Figure 5

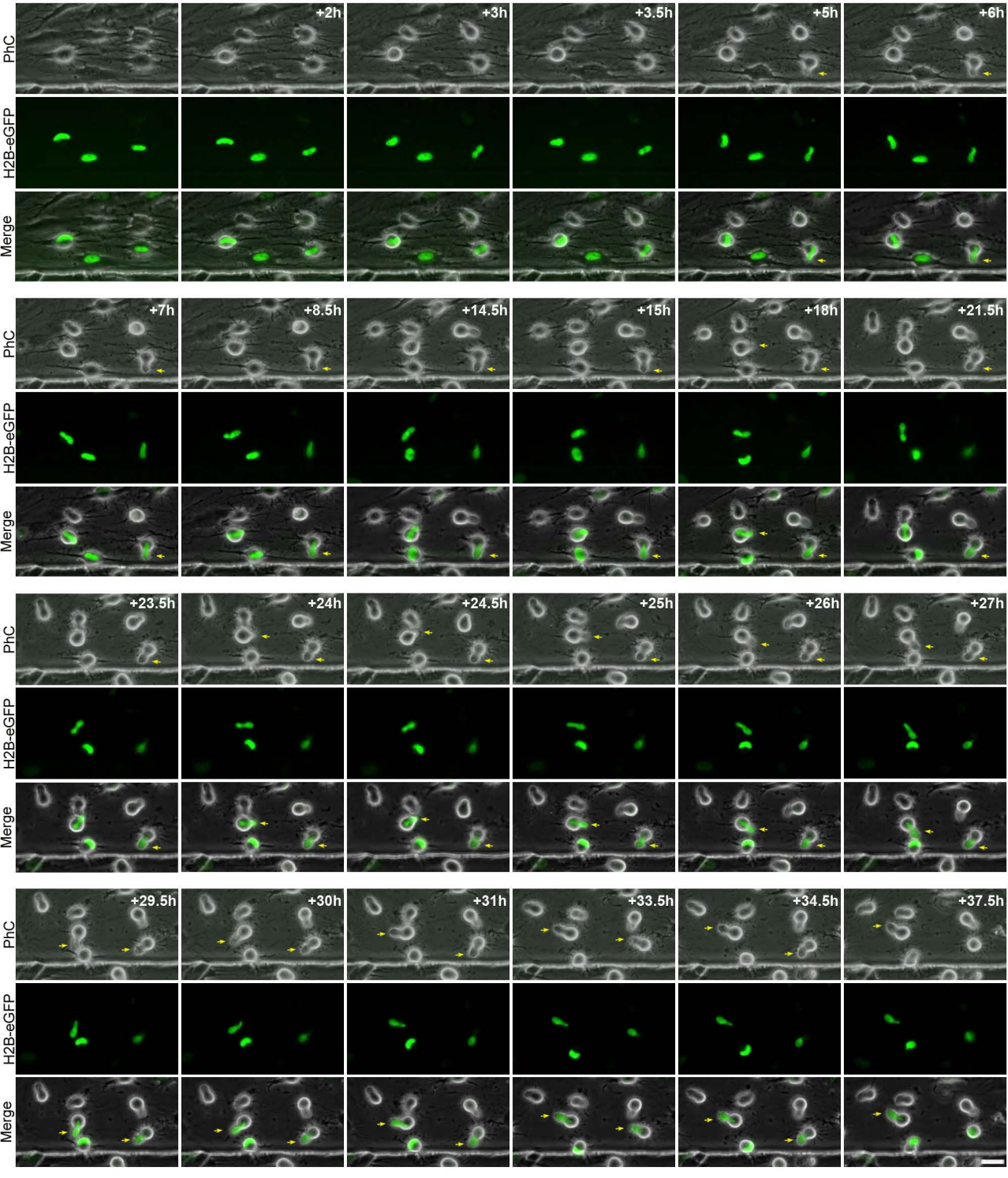
PhC
H2B-eGFP
Merge
+2h
+3h
+3.5h
+5h
+6h
+7h
+8.5h
+14.5h
+15h
+18h
+21.5h
+23.5h
+24h
+24.5h
+25h
+26h
+27h
+29.5h
+30h
+31h
+33.5h
+34.5h
+37.5h

Figure 6

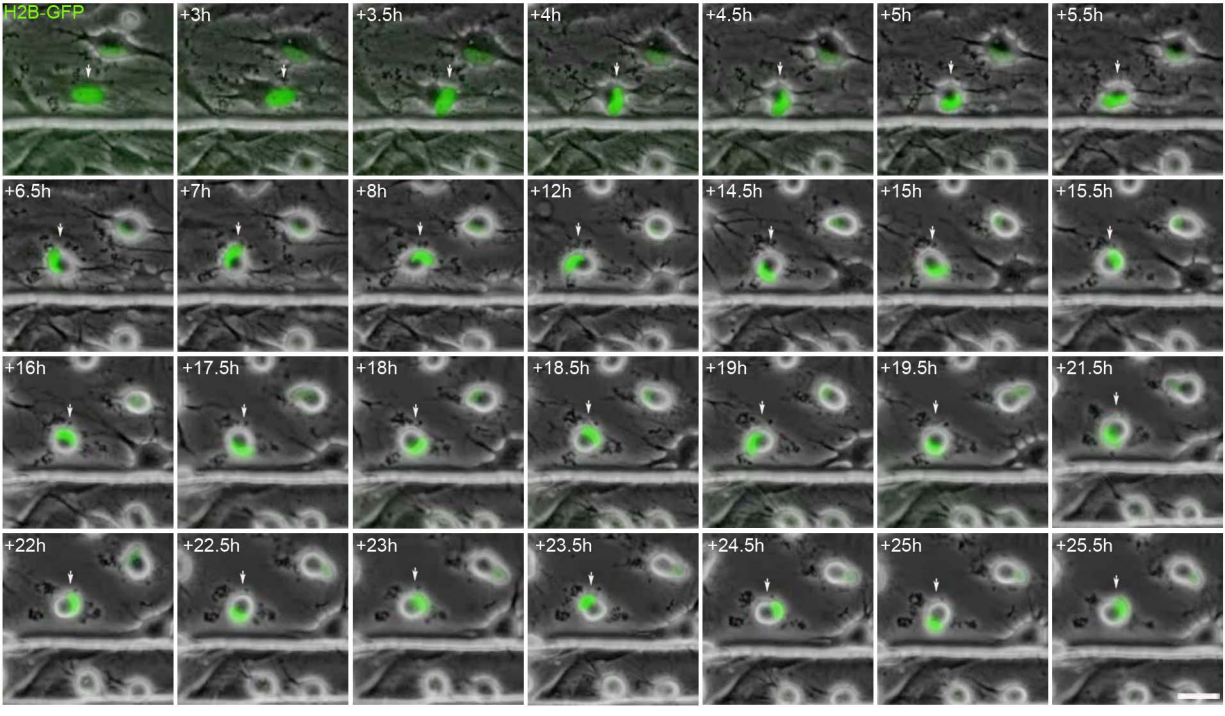
H2B-GFP
+3h
+3.5h
+4h
+4.5h
+5h
+5.5h
+6.5h
+7h
+8h
+12h
+14.5h
+15h
+15.5h
+16h
+17.5h
+18h
+18.5h
+19h
+19.5h
+21.5h
+22h
+22.5h
+23h
+23.5h
+24.5h
+25h
+25.5h

Figure 7

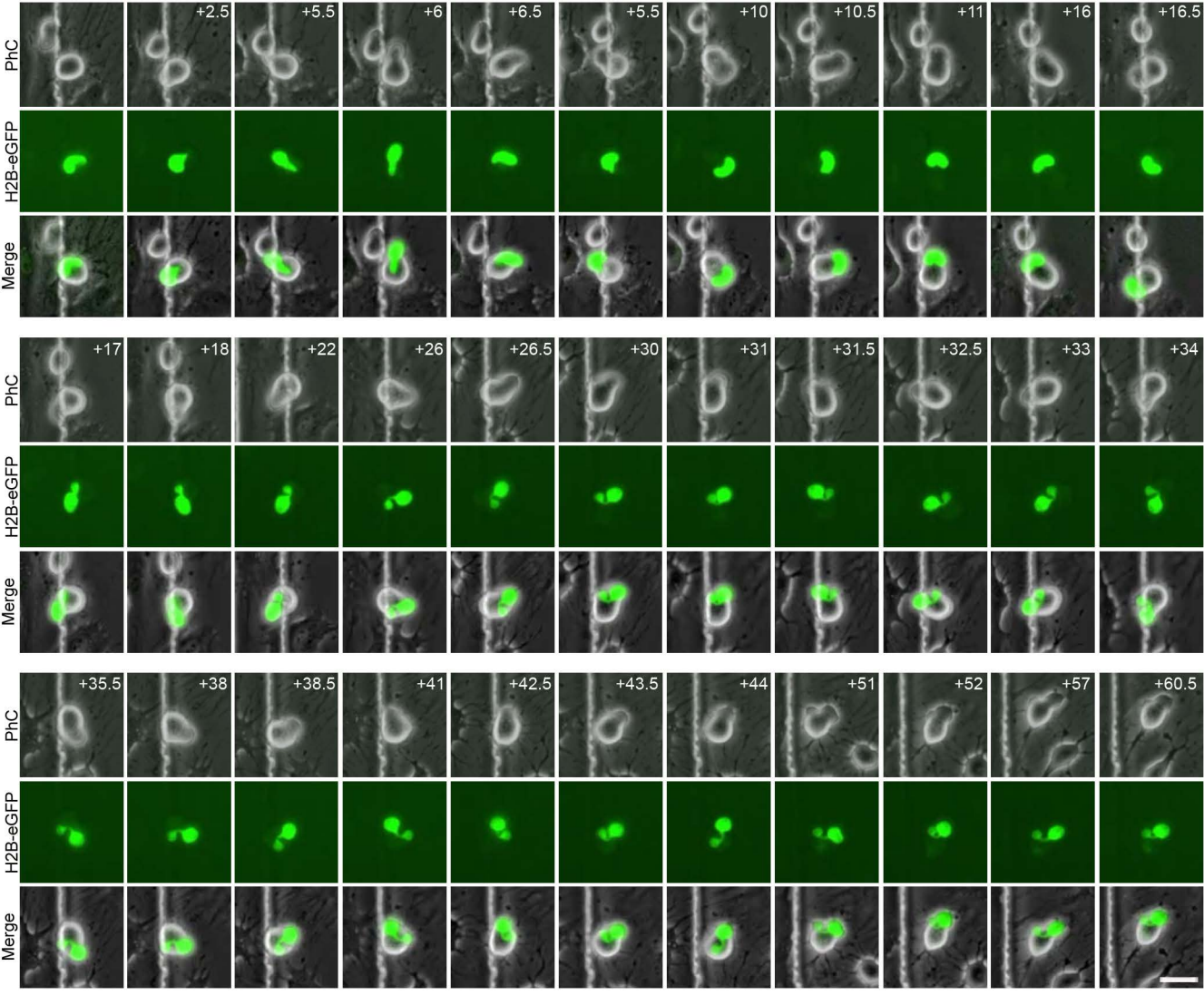
PhC
H2B-eGFP
Merge
+2.5
+5.5
+6
+6.5
+5.5
+10
+10.5
+11
+16
+16.5
+17
+18
+22
+26
+26.5
+30
+31
+31.5
+32.5
+33
+34
+35.5
+38
+38.5
+41
+42.5
+43.5
+44
+51
+52
+57
+60.5

Figure 8

A

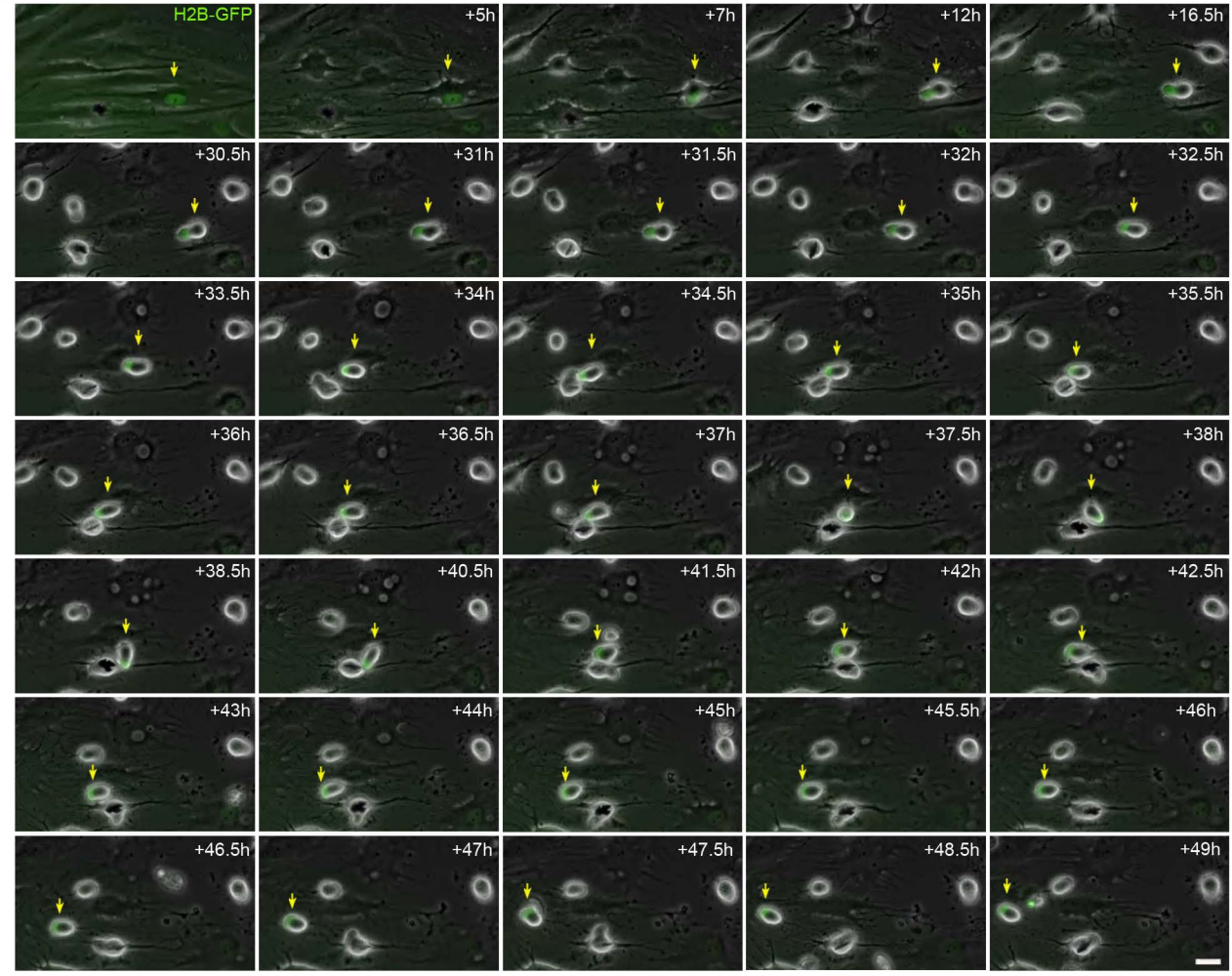
H2B-GFP
+5h
+7h
+12h
+16.5h
+30.5h
+31h
+31.5h
+32h
+32.5h
+33.5h
+34h
+34.5h
+35h
+35.5h
+36h
+36.5h
+37h
+37.5h
+38h
+38.5h
+40.5h
+41.5h
+42h
+42.5h
+43h
+44h
+45h
+45.5h
+46h
+46.5h
+47h
+47.5h
+48.5h
+49h

B

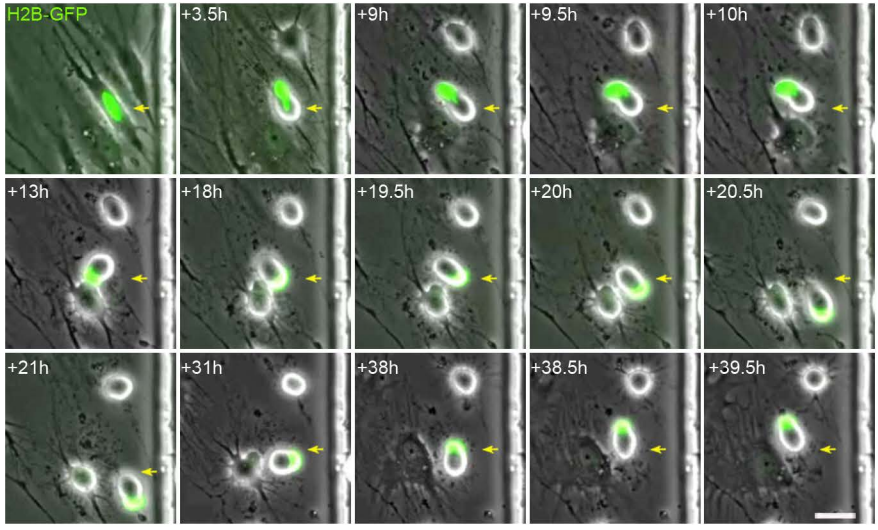
H2B-GFP
+3.5h
+9h
+9.5h
+10h
+13h
+18h
+19.5h
+20h
+20.5h
+21h
+31h
+38h
+38.5h
+39.5h

Figure 9

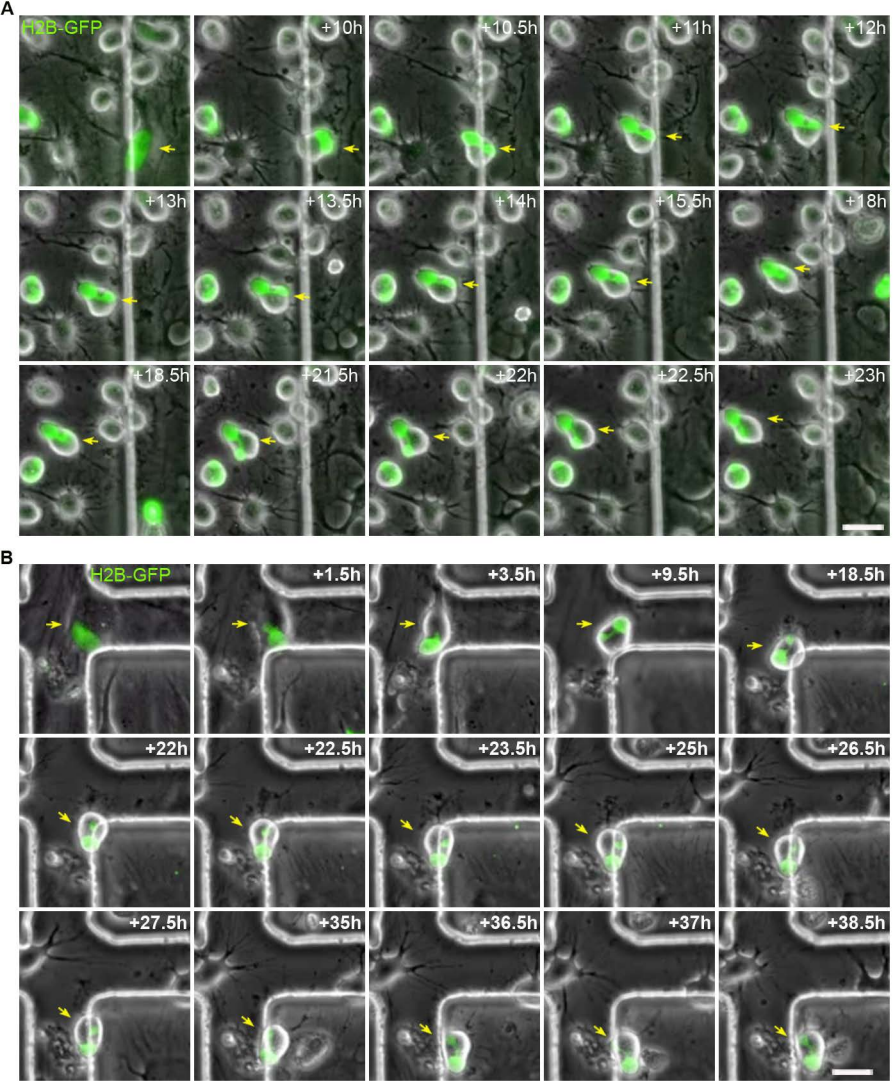
A
H2B-GFP
+10h
+10.5h
+11h
+12h
+13h
+13.5h
+14h
+15.5h
+18h
+18.5h
+21.5h
+22h
+22.5h
+23h
B
H2B-GFP
+1.5h
+3.5h
+9.5h
+18.5h
+22h
+22.5h
+23.5h
+25h
+26.5h
+27.5h
+35h
+36.5h
+37h
+38.5h

Figure10

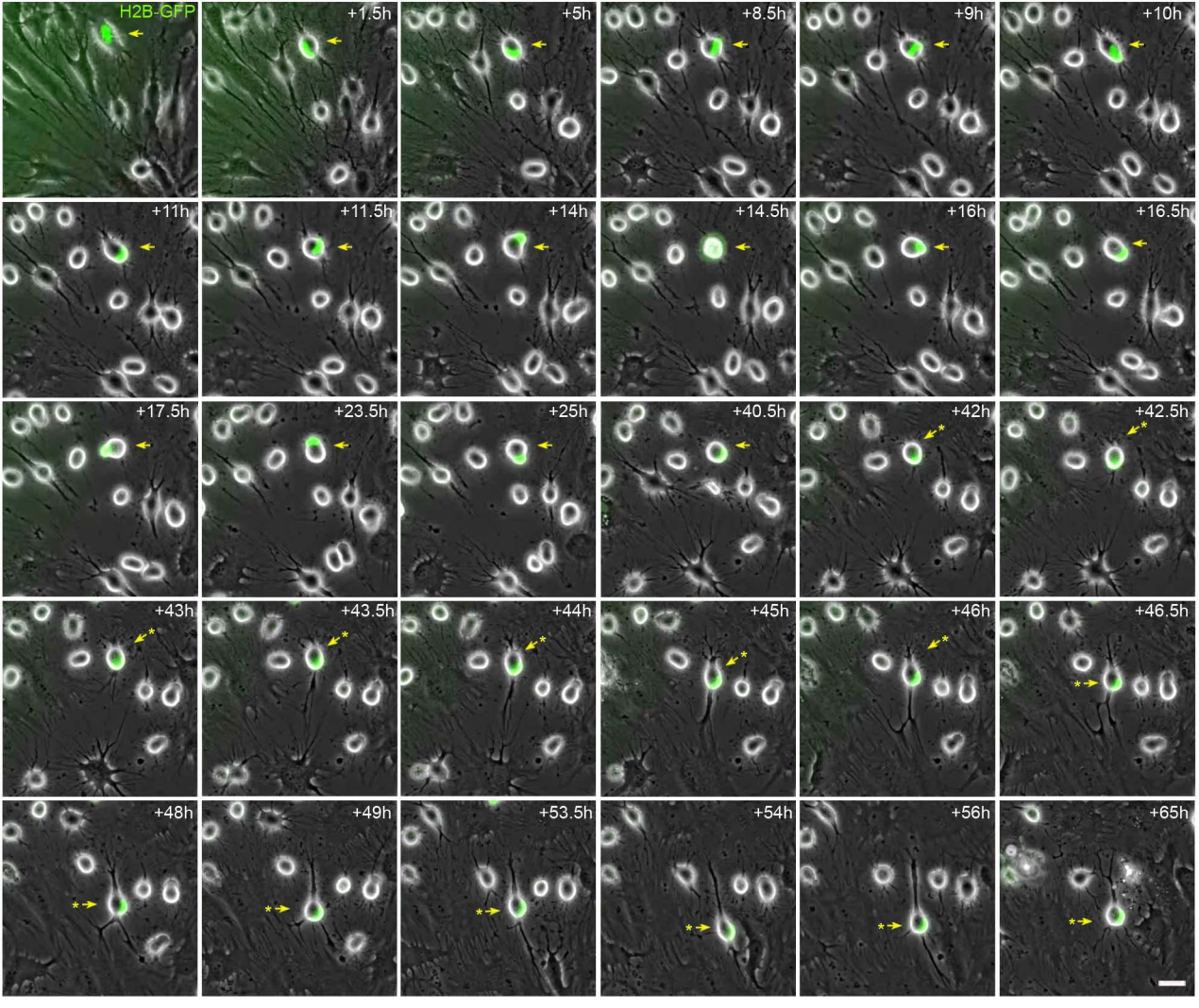
H2B-GFP
+1.5h
+5h
+8.5h
+9h
+10h
+11h
+11.5h
+14h
+14.5h
+16h
+16.5h
+17.5h
+23.5h
+25h
+40.5h
+42h
+42.5h
+43h
+43.5h
+44h
+45h
+46h
+46.5h
+48h
+49h
+53.5h
+54h
+56h
+65h

Figure11

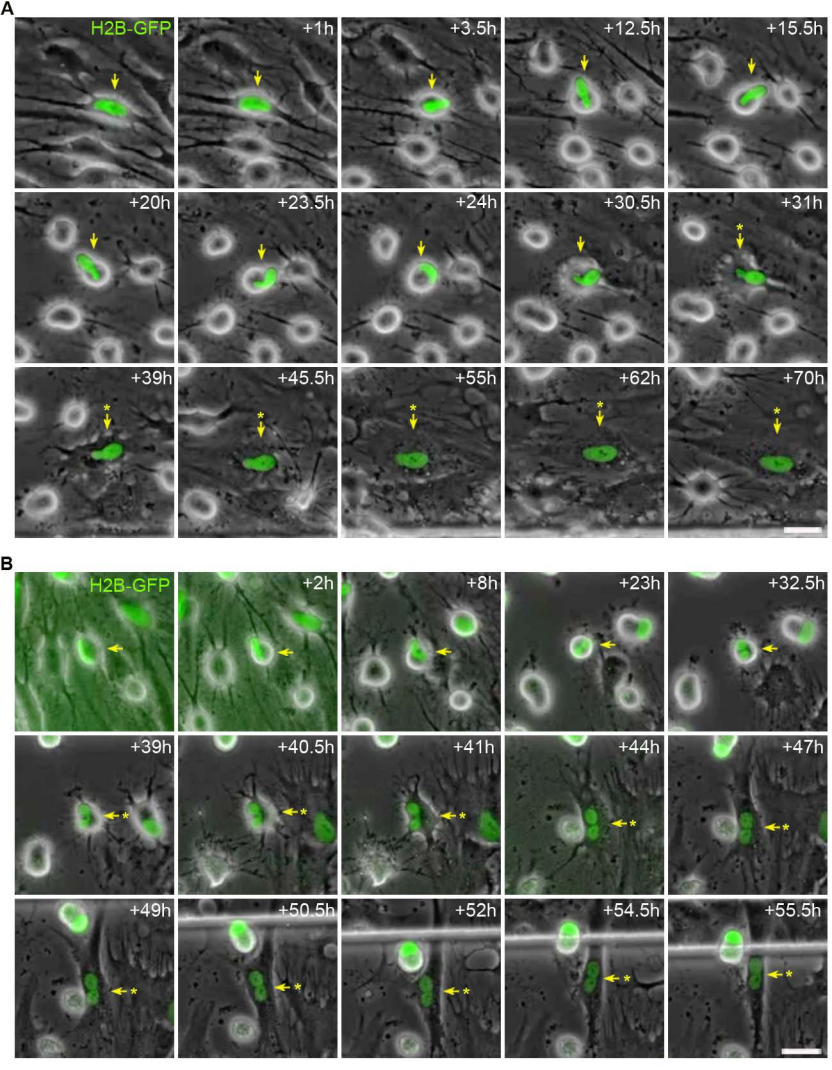
A
H2B-GFP
+1h
+3.5h
+12.5h
+15.5h
+20h
+23.5h
+24h
+30.5h
+31h
+39h
+45.5h
+55h
+62h
+70h
B
H2B-GFP
+2h
+8h
+23h
+32.5h
+39h
+40.5h
+41h
+44h
+47h
+49h
+50.5h
+52h
+54.5h
+55.5h

Figure12

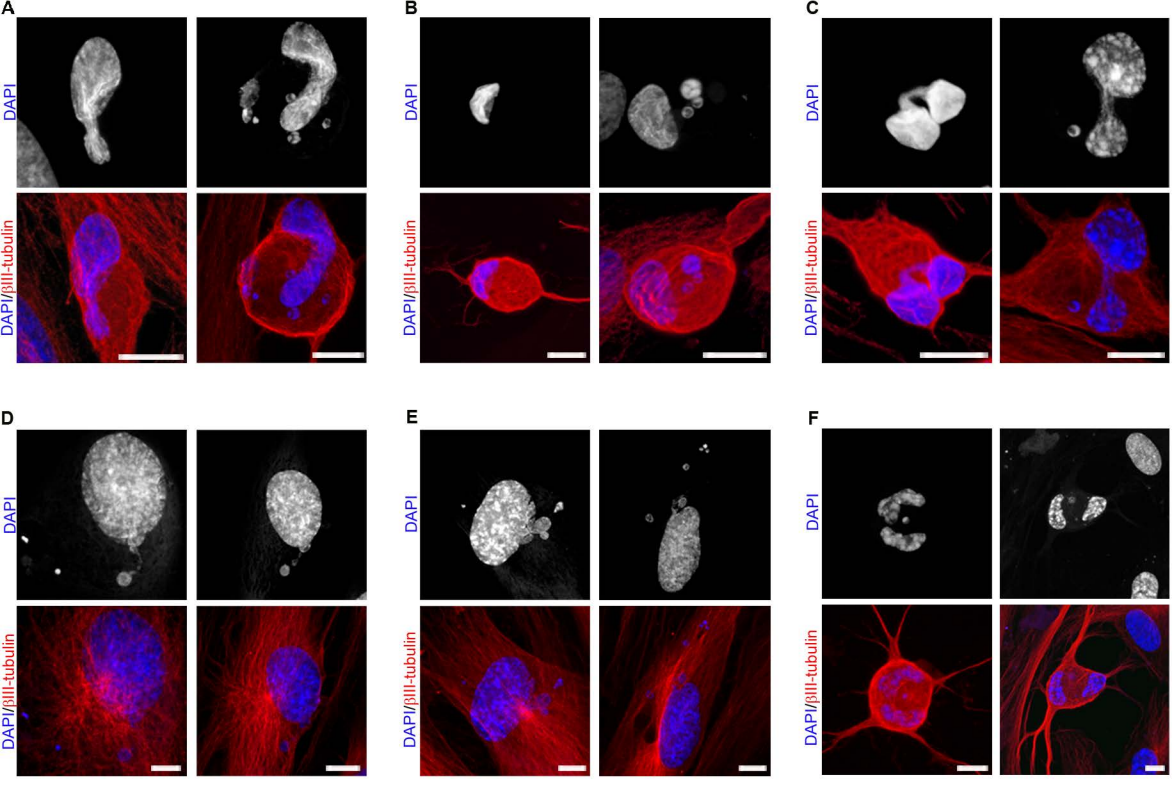

Figure13